



# Distribution of volatile organic compounds over Indian subcontinent during winter: WRF-chem simulation versus observations<sup>\*</sup>



Lakhima Chutia<sup>a</sup>, Narendra Ojha<sup>b,\*</sup>, Imran A. Girach<sup>c</sup>, Lokesh K. Sahu<sup>b</sup>,  
Leonardo M.A. Alvarado<sup>d</sup>, John P. Burrows<sup>d</sup>, Binita Pathak<sup>a,e</sup>, Pradip Kumar Bhuyan<sup>a</sup>

<sup>a</sup> Centre for Atmospheric Studies, Dibrugarh University, Dibrugarh, India

<sup>b</sup> Space and Atmospheric Sciences Division, Physical Research Laboratory, Ahmedabad, India

<sup>c</sup> Space Physics Laboratory, Vikram Sarabhai Space Centre, Thiruvananthapuram, India

<sup>d</sup> Institute of Environmental Physics (IUP), University of Bremen, Bremen, Germany

<sup>e</sup> Department of Physics, Dibrugarh University, Dibrugarh, India

## ARTICLE INFO

### Article history:

Received 7 January 2019

Received in revised form

6 May 2019

Accepted 19 May 2019

Available online 23 May 2019

### Keywords:

South Asia

WRF-Chem

Air quality modeling

Hydrocarbons

VOCs

Satellite retrievals

## ABSTRACT

We investigate the distribution of volatile organic compounds (VOCs) over Indian subcontinent during a winter month of January 2011 combining the regional model WRF-Chem (Weather Research and Forecasting model coupled with Chemistry) with ground- and space-based observations and chemical reanalysis. WRF-Chem simulated VOCs are found to be comparable with ground-based observations over contrasting environments of the Indian subcontinent. WRF-Chem results reveal the elevated levels of VOCs (e. g. propane) over the Indo-Gangetic Plain (16 ppbv), followed by the Northeast region (9.1 ppbv) in comparison with other parts of the Indian subcontinent (1.3–8.2 ppbv). Higher relative abundances of propane (27–31%) and ethane (13–17%) are simulated across the Indian subcontinent. WRF-Chem simulated formaldehyde and glyoxal show the western coast, Eastern India and the Indo-Gangetic Plain as the regional hotspots, in a qualitative agreement with the MACC (Monitoring Atmospheric Composition and Climate) reanalysis and satellite-based observations. Lower values of  $R_{GF}$  (ratio of glyoxal to formaldehyde <0.04) suggest dominant influences of the anthropogenic emissions on the distribution of VOCs over Indian subcontinent, except the northeastern region where higher  $R_{GF}$  (~0.06) indicates the role of biogenic emissions, in addition to anthropogenic emissions. Analysis of HCHO/NO<sub>2</sub> ratio shows a NO<sub>x</sub>-limited ozone production over India, with a NO<sub>x</sub>-to-VOC transition regime over central India and IGP. The study highlights a need to initiate in situ observations of VOCs over regional hotspots (Northeast, Central India, and the western coast) based on WRF-Chem results, where different satellite-based observations differ significantly.

© 2019 Elsevier Ltd. All rights reserved.

## 1. Introduction

Volatile organic compounds (VOCs) are produced in the atmosphere from both natural and anthropogenic sources and play vital roles in the atmospheric chemistry, air quality and climate (Seinfeld and Pandis, 2006). VOCs are involved in the formation of photochemical smog in the presence of oxides of nitrogen (NO<sub>x</sub>), influencing the oxidizing capacity of the troposphere (Atkinson, 2000). In addition, VOCs are precursors of aerosols through gas-to-particle

conversion (Guenther et al., 2012; Piccot et al., 1992). VOCs include a variety of species such as non-methane hydrocarbons (NMHCs) and oxygenated-VOCs (OVOCs) which vary from few parts per trillion by volume (pptv) to several parts per billion by volume (ppbv). The chemical composition of VOCs varies from region to region depending upon sources and therefore speciated information is needed to assess the impact of individual VOC compound. Globally, biogenic emissions are major contributors to the budget of VOCs in the atmosphere as compared to that from anthropogenic sources (e. g. Müller, 1992; Guenther et al., 2006; Seinfeld and Pandis, 2006). In Asian region, India is the second largest (25.2%) contributor to the emission of non-methane VOCs (NMVOCs) after China (35.2%), with residential combustion, on-road transportation, and industries being the major sources in the region (Li et al., 2017).

<sup>\*</sup> This paper has been recommended for acceptance by Dr. Haidong Kan.

<sup>\*</sup> Corresponding author.

E-mail address: [ojha@prl.res.in](mailto:ojha@prl.res.in) (N. Ojha).

Some VOCs are known or suspected carcinogens, e.g. Benzene is considered as Group 1 human carcinogen by the International Agency for Research on Cancer (IARC); while other VOCs (like toluene, ethylbenzene, o-, m-, and p-xylenes) may affect central nervous system, liver, kidneys and the immune system (Filley et al., 2004; Kandiyala et al., 2010). Several studies have reported associations between ambient VOCs and adverse health outcomes through inhalation and ingestion (e.g. Guo et al., 2004; Rumchev et al., 2007 etc.). Glass et al. (2003) reported an increase risk of leukemia and multiple myeloma due to prolonged exposure to benzene. Estimated cancer risk over Kolkata exceeded the threshold value ( $1 \times 10^{-6}$ ) indicating significant cancer risk to the people living in the city (Majumdar et al., 2011). The agencies like US EPA and WHO have not proposed any standard for ambient VOCs due to limited epidemiological and toxicological studies related to VOCs. The Central Pollution Control Board (CPCB) of India has provided regulation guideline for benzene and benzo(a)pyrene by including them in National Ambient Air Quality Standard since November 2009. For the industrial, residential, rural and ecologically sensitive areas, the air quality standard limits for benzene and benzo(a)pyrene are  $5 \mu\text{g}/\text{m}^3$  and  $1 \mu\text{g}/\text{m}^3$ , respectively.

OVOCs from vehicular exhaust, fossil-fuel combustion, solvent usage, industry and biogenic sources (Placet et al., 2000; Sawyer et al., 2000) contribute to a considerable portion of total VOC burden in the troposphere. Formaldehyde (HCHO) and glyoxal (CHOCHO) are two ubiquitous OVOCs which can be used as indicators of fast organic photochemistry in the lower troposphere (Volkamer et al., 2005). HCHO is mostly produced from the oxidation of isoprene ( $\text{C}_5\text{H}_8$ ) and methane ( $\text{CH}_4$ ) by the OH radicals (Arlander et al., 1995). Photolysis and oxidation by OH radicals are major HCHO sinks, resulting in a lifetime of a few hours (Logan et al., 1981). Further, the ratio of HCHO and  $\text{NO}_x$  provides an effective parameter to investigate the  $\text{NO}_x$  vs VOC-limited ozone photochemistry (Martin et al., 2004; Duncan et al., 2010; Chang et al., 2016). Similar to HCHO, CHOCHO is produced from the oxidation of many VOCs, such as isoprene, alkene and aromatic species (Fu et al., 2008). It is the smallest  $\alpha$ -dicarbonyl used as an indicator of SOA formation (Fu et al., 2008; Vrekoussis et al., 2009) with a short atmospheric residence time of the order of a few hours (Atkinson, 2000). Besides the oxidation of primary VOCs, direct emissions from biogenic, biomass-burning and anthropogenic sources also contribute to HCHO and CHOCHO loading in the continental boundary layer (Munger et al., 1995; Lee et al., 1998). Remote sensing of tropospheric HCHO and CHOCHO together with chemistry-transport models have been used to constrain the NMVOC emissions (e.g. Fu et al., 2007; Palmer et al., 2003a).

Studies of VOCs remain limited over the Indian subcontinent, where rapid urbanization, industrialization, and increase in traffic have led to enhanced emissions of VOCs (e.g. Akimoto et al., 2006; De Smedt et al., 2010; Li et al., 2014). In addition, VOC sources in South Asian region are highly variable depending upon the land-use and land cover patterns. Therefore, efforts have been made towards the measurements of ambient VOCs representing distinct environments such as industrial, urban, rural, high altitude etc. of India. Padhy and Varshney (2000) estimated total NMVOC at 13 sites in the urban environment of Delhi during 1994–1995, followed by VOC observations in western India (Srivastava et al., 2000; Sahu and Lal, 2006a, b). In the megacities (e.g. Delhi, Mumbai, Kolkata), very high levels of VOCs were observed in the vicinity of vehicular emissions ( $100\text{--}800 \mu\text{g}/\text{m}^3$ ) and industrial emissions ( $100\text{--}600 \mu\text{g}/\text{m}^3$ ) (Talapatra and Srivastava, 2011). Sinha et al. (2014) reported dominance of OVOCs ( $5.9\text{--}37.5 \text{ nmol mol}^{-1}$ ) at Mohali, a suburban site in north-western India during the pre-monsoon using a Proton Transfer Reaction Mass Spectrometer (PTR-MS). Sahu et al. (2016) used PTR-TOF-MS technique and

observed that methanol ( $17.85 \pm 4.2 \text{ ppbv}$ ) and toluene ( $4.3 \pm 2.3 \text{ ppbv}$ ) are the dominant OVOCs and primary VOCs respectively at an urban site in western India during winter and attributed observed variations in VOCs to meteorology, local emissions, and transport from the Indo-Gangetic Plain (IGP). Measurements of VOCs were also conducted over the lower Himalayan region (Sarkar et al., 2014, 2016; Sarangi et al., 2016; Bhardwaj et al., 2018). Sarkar et al. (2014) showed that vehicle exhausts (60%) and solvent evaporation (18%) were major sources over Darjeeling during post-monsoon. Seasonal cycle of NMHCs at a high-altitude site Nainital in central Himalaya exhibited a maximum in late autumn/early winter and minimum during monsoon (Sarangi et al., 2016). Levels of light NMHCs were observed to be significantly higher in Kathmandu valley than those at Nainital (Bhardwaj et al., 2018).

Aforementioned summary of VOC studies in India reveals large variability in the mixing ratios of VOCs over South Asia, however, these observations limited in space and time remain insufficient to derive the distribution over the entire Indian subcontinent and to compare different sub regions of diverse meteorology and emissions. Modeling studies that could fill this gap have been lacking evaluations against in situ observations over this region (e.g. Pozzer et al., 2010). Here, we study the distribution of some of the important VOCs by combining a regional model WRF-Chem, ground-based and satellite-based measurements, and MACC reanalysis during winter (January 2011). The study period (winter) is chosen as VOC levels are relatively higher due to accumulation in shallower boundary layer and lesser photochemical loss due to lower OH concentrations (Laban et al., 2018). Moreover, observations for a greater number of stations were available during this season and provide better dataset for the comparison with model.

Manuscript is structured as follows: Section 2 presents the description of WRF-Chem set up including the schemes to simulate physical and chemical processes, and different inputs to the model. Various datasets viz., ground-based measurements, satellite retrievals and reanalysis are described in section 3. Section 4.1 presents the analysis of WRF-Chem results and comparison with in situ data, and the comparisons with satellite-based observations and MACC reanalysis are presented in section 4.2, followed by evaluation of HCHO/ $\text{NO}_2$  ratio to investigate sensitivity of ozone to VOCs and  $\text{NO}_x$  in section 4.3. A summary of the study and main conclusions are presented in section 5.

## 2. Model description

Weather Research and Forecasting (WRF) model coupled with chemistry (WRF-Chem) (Grell et al., 2005) version 3.9.1.1 is used in the present study. Model domain (Fig. 1) is centered at  $21^\circ\text{N}$  and  $82^\circ\text{E}$  and the horizontal resolution is  $12 \text{ km} \times 12 \text{ km}$ .

Initial and boundary conditions for meteorological and chemical fields are taken from ERA-interim reanalysis and MOZART4-GEOS5 (Emmons et al., 2010) respectively. The schemes for parameterization of various processes (Table 1) are based on earlier evaluation and applications of this model over Indian region (e.g. Kumar et al., 2012a, b; Girach et al., 2017). We have used a recent version (3.9.1.1) of the WRF-Chem model and performed a high-resolution ( $12 \text{ km} \times 12 \text{ km}$ ) simulation using updated anthropogenic emission inventory: Emissions Database for Global Atmospheric Research - Hemispheric Transport of Air Pollution (EDGAR-HTAP) v2 as compared to the previous studies.

Regional Acid Deposition Model version 2 (RADM2) (Stockwell et al., 1990) coupled with the Modal Aerosol Dynamics for Europe (MADE) (Ackermann et al., 1998) and the Secondary Organic Aerosol Model (SORGAM) (Schell et al., 2001) have been used to simulate the chemical processes. Anthropogenic emissions are

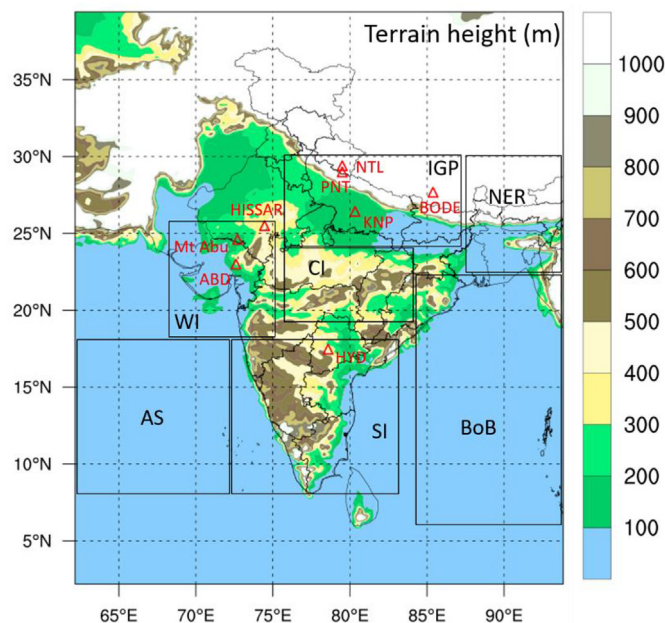


**Fig. 1.** Simulation domain showing terrain height (meter), defined regions (black rectangles) and observation sites (red triangles) over Indian subcontinent. (For interpretation of the references to color in this figure legend, the reader is referred to the Web version of this article.)

based on the EDGAR-HTAP inventory (Janssens-Maenhout et al., 2015), which includes NMVOCs, CO, SO<sub>2</sub>, NO<sub>x</sub>, NH<sub>3</sub>, PM<sub>10</sub>, PM<sub>2.5</sub>, BC and OC at a horizontal resolution of 0.1° × 0.1°. Emissions of several NMVOCs are available in the EDGAR-HTAP inventory following the REanalysis of the TROpospheric chemical composition (RETRO). These individual (or lumped) species are then mapped to the chemical species in the RADM2 chemical mechanism. Biomass burning emissions are included from the Fire INventory from NCAR (FINN) (Wiedinmyer et al., 2011). Biogenic emissions are calculated online in WRF-Chem using the Model of Emissions of Gases and Aerosols from Nature (MEGAN) (Guenther et al., 2006).

### 3. Study region and dataset

#### 3.1. Study region

Based on the topography, meteorology, emissions, land use and land cover, Indian subcontinent has been divided into following sub regions: Indo-Gangetic Plain (IGP: 24–30°N; 76–87°E), North East Region (NER: 22–30°N; 88–94°E), Central India (CI: 19–24°N; 76–84°E), West India (WI: 18–26°N; 68–75°E), Southern Indian peninsula (SI: 8°–18°N; 72–83°E), and marine regions: Bay of Bengal (BoB: 6–22°N; 84–94°E) and Arabian Sea (AS: 8–18°N;

62–72°E) (Fig. 1). IGP covers about 21% of Indian land mass and is one of the most densely populated regions of the world with strong anthropogenic emissions (e.g. Nair et al., 2007). NER parts are forest covered and the population is involved in agricultural activities, however, biomass-burning, brick kilns, oil and gas fields have made NER vulnerable to enhanced pollution especially during winter (Gogoi et al., 2017; Pathak et al., 2016). CI constitutes 12.30% of the forest area of India and agricultural residue burning activities are among major emission sources here (Sahu et al., 2015). WI is an industrialized region with larger urban population (Census of India, 2011). SI is influenced by anthropogenic emissions from urban hotspots and regional biomass-burning. BoB is surrounded by densely populated and industrialized regions in north, west and east and receives strong continental outflow during winter (e.g. Ojha et al., 2012; Kumar and Verma, 2016; Verma et al., 2017; Priyadharshini et al., 2018). AS is influenced by the transport from Indian subcontinent and from far distant regions of the Middle East (e.g. Moorthy et al., 2005).

#### 3.2. Ground-based dataset

Light NMHCs such as ethane, ethene, propane, and propene were measured using GC-FID instrument. In GC-FID, samples are pre-concentrated in a cryo-trap at liquid nitrogen temperature. The adsorbed NMHCs were then heated to 100 °C and transferred into the GC column where temperature was ramped from 0 to 200 °C in steps to separate different NMHCs. A detailed description of GC-FID based analysis is available in earlier studies (e.g. Sahu and Lal, 2006a, b; Sarangi et al., 2016). In recent years, PTR-MS technique has been used for online measurements of VOCs. In this technique, VOC species with a proton affinity greater than water are ionized by the transfer of proton from reagent hydronium (H<sub>3</sub>O<sup>+</sup>) ions and the products are detected using a TOF or quadrupole mass spectrometer (Lindinger et al., 1998). A detailed description of the PTR-MS observations in India is presented in Sinha et al. (2014) and Sahu et al. (2016). Present study uses ground-based VOC data measured at 8 different stations (Fig. 1) over the Indian subcontinent: Nainital (Sarangi et al., 2016); Pantnagar (Sarangi et al., 2016); Bode (Bhardwaj et al., 2018); Kanpur (Lal et al., 2012); Hissar (Lal et al., 2012); Mt Abu (Sahu and Lal, 2006b); Ahmedabad (Lal et al., 2012) and Hyderabad (Venkanna et al., 2015).

#### 3.3. Satellite data

Satellite-based observations of formaldehyde (HCHO) and glyoxal (CHOCHO) from the Ozone Monitoring Instrument (OMI), the Global Ozone Monitoring Experiment-2 (GOME-2) and Scanning Imaging Absorption spectroMeter for Atmospheric CHartography (SCIAMACHY) have been analyzed. OMI onboard Aura is a nadir-viewing imaging spectrometer, which measures solar backscatter in the near-UV/Visible (270–500 nm) (Levelt et al., 2006).

**Table 1**

List of schemes used to parameterize the different processes in the WRF-Chem model.

Processes	Scheme	References
Microphysics	Lin microphysics scheme	Lin et al. (1983)
Long wave radiation	Rapid Radiative Transfer Model (RRTM)	Mlawer et al. (1997)
Shortwave radiation	Goddard Short wave scheme	Chou and Suarez (1994)
Surface layer	Monin-Obukhov (Janjic) scheme	Janjic (1996)
Land surface	Unified Noah land-surface model	Chen and Dudhia (2001)
Boundary Layer	Mellor-Yamada-Janjic scheme	Janjic, 2002
Cumulus parameterization	Grell 3D ensemble scheme	Grell (1993); Grell and Devenyi (2002)
Gas-phase chemical mechanism	RADM2	Stockwell et al. (1990)
Aerosol module	MADE SORGAM	Ackermann et al. (1998); Schell et al. (2001)

OMI provides global coverage everyday with spatial resolution of 13 km × 24 km at nadir and equatorial overpasses at 13:45 LT. GOME-2 onboard MetOp-A and MetOp-B are nadir-viewing UV/visible (240–790 nm) spectrometers (EUMETSAT; European Organization for the Exploitation of Meteorological Satellites) (Callies et al., 2000; Munro et al., 2006). It has spatial resolution of 40 km × 80 km and near global coverage is achieved every day. Since MetOp-B was launched in 2012, the observations from GOME-2/MetOp-A (GOME-2A) only are available for the study period. SCIAMACHY (Burrows et al., 1995; De Smedt et al., 2008) mounted on the ENVISAT satellite. SCIAMACHY, an enhanced version of the GOME, was an 8-channel grating spectrometer covering ultraviolet, visible and near infrared (240–2380 nm) at moderate spectral resolution (0.2 nm–1.5 nm) and overpasses the equator at 10:00 LT, which is about half an hour earlier than GOME. It performs measurements in nadir, limb, and solar/lunar occultation.

Level 3 monthly tropospheric HCHO (OMI and GOME-2A version 14; SCIAMACHY version 12) and CHOCHO (OMI, GOME-2A and SCIAMACHY version 1.5) data with grid size of 0.25° × 0.25° (De Smedt et al., 2008, 2010; 2015; Alvarado et al., 2014) are used here. Tropospheric HCHO and CHOCHO columns were obtained from <http://h2co.aeronomy.be> and [http://www.iup.uni-bremen.de/doas/glyoxal\\_data.htm](http://www.iup.uni-bremen.de/doas/glyoxal_data.htm), respectively. DOAS (differential optical absorption spectroscopy) algorithm is employed for the retrieval of these species eliminating the contributions from interfering species (e. g. O<sub>3</sub>, NO<sub>2</sub>, water vapor, liquid water, etc.). For glyoxal vertical columns (VC), the overall monthly uncertainty in the selected region during January 2011 is given by following equation.

$$\text{Uncertainty} = \alpha \times \text{VC}_{\text{CHOCHO}}^{\text{observed}} + 1 \times 10^{14} \text{molec cm}^{-2},$$

Where  $\alpha$  varies in the range of 10–30%.

### 3.4. MACC reanalysis

O<sub>3</sub>, CO, NO<sub>x</sub>, and HCHO data are obtained from the Monitoring Atmospheric Composition and Climate (MACC) reanalysis and used for comparison with WRF-Chem results. MACC was developed in the precursor project GEMS (Global and regional Earth-system (Atmosphere) Monitoring using Satellite and in-situ data), and is an extension of European Center for Medium range Weather Forecasting (ECMWF) Integrated Forecast System (IFS) coupled with the Model for Ozone and Related chemical Tracers (MOZART) chemistry transport model. Combining both atmospheric modeling and observational data, it provides retrospective analysis product for global chemical composition since year 2003 onwards. We have used the MACC reanalysis data available at a horizontal resolution of 0.25° × 0.25° in the present study. Detailed description of the MACC reanalysis is presented in Inness et al. (2013).

## 4. Results and discussion

WRF-Chem simulated meteorology, dynamics, together with ozone, CO, and NO<sub>x</sub> over South Asia have been evaluated in previous studies (e. g. Kumar et al., 2012a, b). Therefore, in this paper we include discussion on these aspects only briefly (Supplementary material: Tables S1–S3, and Figs. S1–S2) to present model results due to few updates in the model set up (e.g. a recent model version-3.9.1.1, updated anthropogenic emissions based on EDGAR-HTAP, and a different convection scheme- Grell 3D). WRF-Chem simulated temperature, wind pattern, relative humidity, and boundary layer height show a good agreement with the ERA-interim reanalysis (Fig. S1). The percentage differences between WRF-Chem and

ERA-interim varied in the ranges of 0.1–0.5% for temperature, 0.7–7% for relative humidity and 15–35% for planetary boundary layer over different sub-regions in India (Table S1).

WRF-Chem simulated distributions of O<sub>3</sub>, CO, and NO<sub>x</sub> are seen to be generally consistent with the observations (Fig. S2, Table S2 in supplement) as well as previous modeling studies (e.g. Kumar et al., 2012b; Ojha et al., 2012). Further, WRF-Chem simulated distribution of trace gases (O<sub>3</sub>, CO, and NO<sub>x</sub>) show a general agreement with MACC reanalysis (Fig. S2 and Table S3), and typical features of elevated CO and NO<sub>x</sub> over IGP and strong ozone outflow over marine regions are captured. WRF-Chem shows elevated CO (>600 ppbv) over the entire IGP due to strong anthropogenic emissions and lower mixing depth during winter. Overall, we find that WRF-Chem successfully reproduced the distribution and key features of trace gases over Indian region. Moreover, absolute levels of trace gases are also simulated in a manner consistent with previous modeling studies in this region (e.g. Kumar et al., 2012b; Sharma et al., 2017). In following section, the distribution of VOCs based on WRF-Chem simulations is analyzed and the model results are compared with ground based in situ measurements and satellite-based observations.

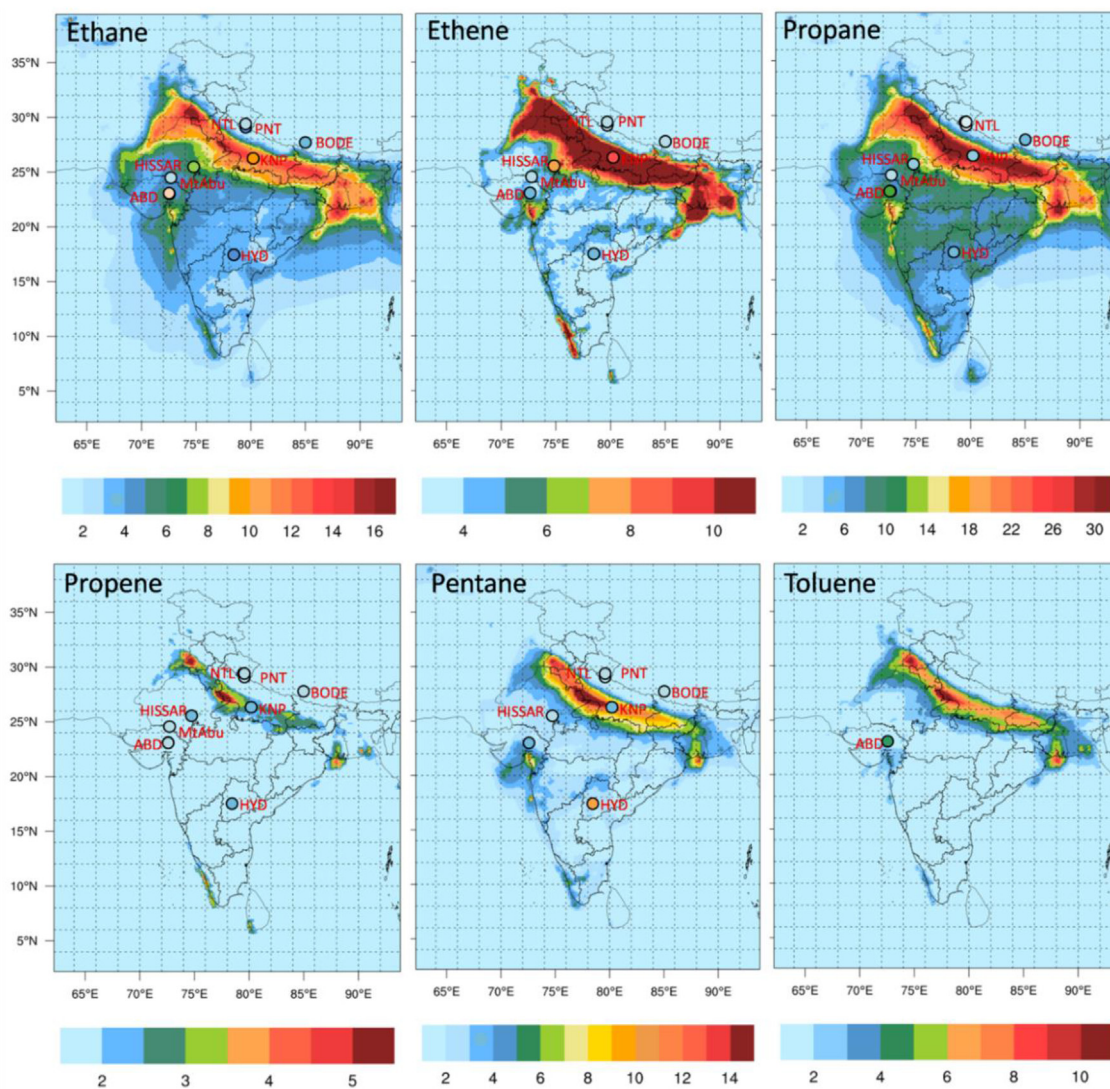
### 4.1. Distribution of VOCs and comparison with in situ measurements

Fig. 2 shows WRF-Chem simulated mean distribution of ethane, ethene, propane, propene, pentane, and toluene during January 2011, superimposed with available in situ observations for winter. WRF-Chem simulation shows high mixing ratios of all these species (e. g., ethane: 10–16 ppbv, propane: 14–30 ppbv) over the IGP region. Besides the IGP, two more regional hotspots of ethene (10 ppbv and above) and propane (14–20 ppbv) are found over the western India and western coast of the southern India in the WRF-Chem simulation. Pentane and toluene exhibit a patch of elevated levels (14 and 8 ppbv, respectively) over the southwestern part of the Uttar Pradesh around Agra (a major world tourist destination in India).

Mean bias (MB), mean normalized bias (MNB) and root-mean-square error (RMS) computed using observed and WRF-Chem simulated VOCs over Indian subcontinent during winter are presented in Table 2.

WRF-Chem underestimates observed ethane at Ahmedabad, Hissar and Hyderabad with MB ranging from –0.8 to –2.8 ppbv and overestimates the measurements at rest of the stations with MB ranging from 0.7 to 2.1 ppbv. The estimated MNB for ethane ranges from 0 to 100% and RMS varies between 0 and 2.8 over the observation sites. Unsaturated NMHCs like ethene and propene show similar behaviour with the underestimations for Hissar (MB –1.5 to –2.8 ppbv) and Hyderabad (MB of –1.2 to –2 ppbv). However, statistical matrices for ethene were typically higher (RMS varies between 2.7 and 3.9) than that of propene (RMS varies between 0.1 and 0.4) at mountain sites. Propane is overestimated by the model with MB ranging from 2 to 21 ppbv over cleaner high-altitude sites as well as urban stations. The measurements of acetone, acetaldehyde, and toluene during winter are available only for Ahmedabad station and these VOCs are reasonably well simulated by WRF-Chem (with MNB ranging from –2.4–28.6%). On the other hand, except at Hyderabad modeled pentane shows an overestimation of 33.3–212.5% at all observed sites.

Further, the relative abundances of VOCs at different stations from WRF-Chem simulation are compared with observations in Fig. 3. Here five species, which were measured at all the stations, are considered for the comparison. Propane is observed to be more abundant over Indian sites with its contribution up to 35–40% at urban location in western India and in Kathmandu valley, in



**Fig. 2.** WRF-Chem simulated monthly average mixing ratios of different VOCs (ppbv) during January 2011. Observations at different sites (circles) are shown on same color scale for comparison. (For interpretation of the references to color in this figure legend, the reader is referred to the Web version of this article.)

agreement with WRF-Chem results. The contributions of ethane at Ahmedabad were 29% and 17% obtained from observation and WRF-Chem, respectively. Propene is typically simulated to be less abundant over all the sites (less than 6%), which agrees with observations, however large discrepancy is seen over Nainital where observations show its contribution higher by a factor of 3. Composition of VOCs in urban Kathmandu valley (Bode) is well reproduced, where propane followed by ethane and ethene are the most abundant species.

The differences in the relative abundances of VOCs are related to different local–regional emissions, transport effects, and chemical lifetimes of individual species. While, transport is the major source at high altitude stations (Mt. Abu and Nainital) and hence these sites exhibit higher contributions of relatively long-lived VOCs (Sarangi et al., 2016). On the other hand, local emissions and transport from the IGP influence Ahmedabad resulting in higher propane and ethane (e. g. Sahu and Lal, 2006a; Sarangi et al., 2016). The differences between model and observation particularly at high-altitude and urban stations could be associated with 1) inadequately resolved topography due to forests, hills and mountains within small areas and 2) uncertainties in the input

anthropogenic emissions, respectively. An attempt to reduce the effect of first factor has been made by conducting model simulations at finer spatial resolution ( $12\text{ km} \times 12\text{ km}$ ). However, the uncertainties in the input for anthropogenic emissions remain significant over the Indian subcontinent (e.g. Li et al., 2017; Huang et al., 2017) mainly arising from the lack of spatially resolved basic activity data as well as missing sources of NMVOCs and that the model computed distributions of trace gases driven by different input emissions were found to differ significantly (Sharma et al., 2017). The inaccurate mapping between species in inventories and models (chemical speciation) may also induce uncertainties (e.g. Fu et al., 2013; Li et al., 2014). Previous studies have also shown large uncertainties in modeled VOCs over this region (Mahajan et al., 2015; Pozzer et al., 2010). Typically, overestimations of some VOCs could be related to the speciation of lumped VOC emissions. Therefore, more experiments are needed to develop representative speciation factors for South Asian region to reduce the associated model–observation differences, in future.

We have analyzed WRF-Chem results to compare the level, regional contributions and composition of VOCs among different sub-regions (Table 3 and Fig. 4). Mean values of different VOCs

**Table 2** Mean bias (MB) in ppbv, mean normalized bias (MNB) in % and root-mean-square error (RMS) computed using observed and WRF-Chem simulated VOCs over Indian subcontinent during winter.

VOCs (ppbv)	Ahmedabad			Mt Abu			Bode			Nainital			Pantnagar			Hissar			Kanpur			Hyderabad		
	MB	MNB	RMS	MB	MNB	RMS	MB	MNB	RMS	MB	MNB	RMS	MB	MNB	RMS	MB	MNB	RMS	MB	MNB	RMS	MB	MNB	RMS
Ethane	-0.8	-9.19	0.8	2.1	100	2.1	1.1	50	1.1	0	0	0	-2.8	-35.44	2.8	1.2	12.63	1.2	-1.1	-24.44	1.1	-1.1	-24.44	1.1
Ethene	3.3	70.21	3.3	2.8	560	2.8	3.9	433.3	3.9	2.7	90	2.7	-2.8	-37.33	2.8	4.8	54.54	4.8	-1.2	-27.90	1.2	-1.2	-27.90	1.2
Propane	7.2	60	7.2	6.2	885.7	6.2	7.1	887.5	7.1	9.6	600	9.6	5.9	190.32	5.9	21	538.46	21	2	43.47	2	2	43.47	2
Propene	0.3	21.42	0.3	0	100	0	0.1	10	0.1	0	0	0	-1.5	-65.21	1.5	0.2	9.09	0.2	-2	-76.92	2	-2	-76.92	2
Pentane	6.2	187.87	6.2	0.5	55.55	0.5	1.7	212.5	1.7	1.1	47.8	1.1	0.6	33.33	0.6	4.8	154.83	4.8	-8.1	-79.41	8.1	-8.1	-79.41	8.1
Acetaldehyde	1.4	28.57	1.4	-	-	-	-	-	-	-	-	-	-	-	-	-	-	-	-	-	-	-	-	-
Acetone	-0.4	-7.54	0.4	-	-	-	-	-	-	-	-	-	-	-	-	-	-	-	-	-	-	-	-	-
Toluene	-0.1	-2.38	0.1	-	-	-	-	-	-	-	-	-	-	-	-	-	-	-	-	-	-	-	-	-

computed by averaging the values at all grid points in the particular sub-region are given in Table 3. Relative percentage contributions of different VOCs to the total VOC simulated among different sub-regions are also presented in Table 3. We have summed up each of the VOCs over different sub regions to calculate the total modeled VOCs. The mean levels of VOCs are simulated to be the highest over the IGP, particularly of ethene ( $8.3 \pm 6.8$  ppbv), propane ( $16 \pm 11.8$  ppbv), pentane ( $5.1 \pm 5.5$  ppbv) in comparison of their respective levels of 2–4.4, 4.6–9.1, 1.3–2.7 ppbv, respectively over other parts of India. Total modeled ethane summed over the model domain during January 2011 is estimated as 27 ppbv. Ethane levels are found to be highest over IGP ( $6.9 \pm 4.2$  ppbv) which accounts 25% to the total modeled ethane. The percentage contributions of ethane relative to the total simulated ethane are found to be 19.1%, 12.9%, 16.2%, 10% over NER, CI, WI, SI respectively. WRF-Chem result shows elevated VOC levels over NER region next to IGP. NER includes the Bangladesh region, and that the higher VOC loadings seen here have effects from sources in the Bangladesh, as well as in eastern parts of the IGP. In particular, ethane (5.3 ppbv, 19.1% to the total modeled ethane), ethene (4.4 ppbv, 19.3% to the total), propane (9.1 ppbv, 18.3% to the total), and toluene (1.8 ppbv, 20.6% to the total) are simulated to be higher over the NER. The VOC contributions over oceanic regions are less than 10%. WRF-Chem results reveal that the sum of these non-methane VOCs is highest over IGP (37.8 ppbv), followed by the NER (21.8 ppbv). This finding is further corroborated in the next section (Section 4.2) by analyzing the formaldehyde and glyoxal from model and satellite-based observations. Over Indian landmass, propane (40–44%) followed by ethane (18–26%) and ethene (17–22%) show greater contributions, while propene (3–5%) is less abundant (Fig. 4). Due to their longer atmospheric lifetimes and higher global abundance, propane and ethane contributions are higher compared to the reactive species like ethene, propene etc. (Sahu and Lal, 2006b). Composition over the oceanic region is simulated to be different with higher contribution of ethane (39–54%). Composition of VOCs is distinct over ocean due to the influences of biogenic oceanic emissions (Dixon et al., 2013a; Fischer et al., 2012) besides the wintertime strong continental outflow from the Indian subcontinent (e.g. Lawrence and Lelieveld, 2010; Ojha et al., 2012).

Enhanced VOC loading over the IGP is attributed to strong anthropogenic emissions in the region from industrial sources, biomass burning, power plants and vehicular emissions (Lal et al., 2012; Sarkar et al., 2016). In contrast, transport effects, and local to regional sources including those in the Bangladesh lead to elevated VOCs over the NER. Model predicts lower levels of VOCs over the oceanic regions as compared to the Indian landmass. As presented in Table 3, higher VOC loading over the Bay of Bengal than those over the Arabian Sea are attributed to stronger South Asian outflow during the winter.

#### 4.2. Formaldehyde (HCHO) and glyoxal (CHOCHO)

Spatial distribution of surface HCHO simulated by WRF-Chem model is compared with the MACC reanalysis during January 2011 in Fig. 5 and a summary of the comparison for different sub-regions is presented in Table 4.

WRF-Chem simulated HCHO levels are in the range of 1–5 ppbv over Indian subcontinent and surround oceanic regions and show good spatial correlations ( $r = 0.69–0.95$ ) with the MACC reanalysis except for CI ( $r = 0.27$ ). The mean mixing ratios are generally in agreement between the WRF-Chem and MACC reanalysis, with relatively better agreement (lower biases) over the hotspot regions IGP (MB = -0.2) and the NER (MB = 0.4) (Table 4). However, WRF-Chem overestimated the MACC reanalysis by 0.8–1 ppbv over the CI and SI. Such overestimations in HCHO column were also reported

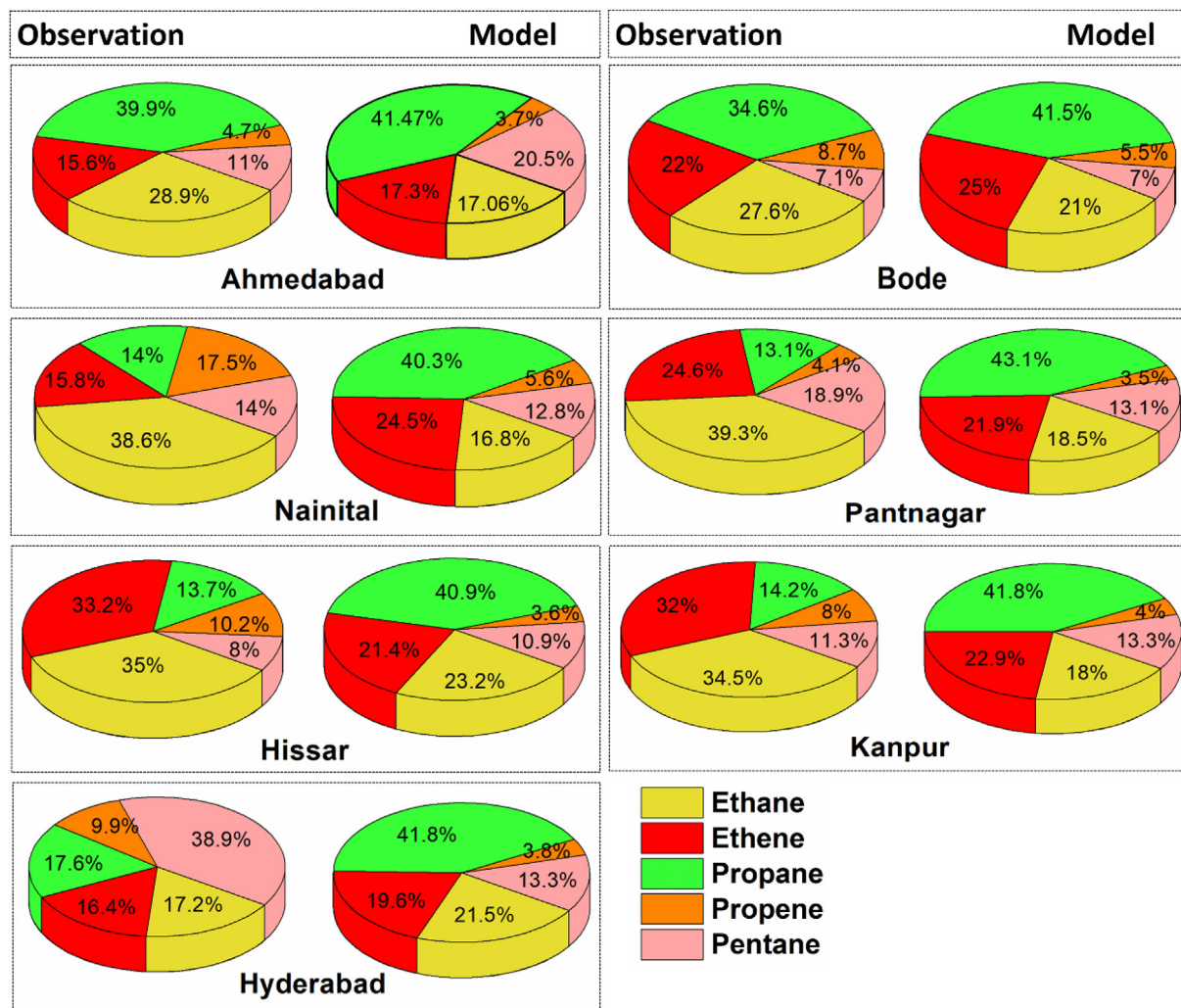


Fig. 3. A comparison of WRF-Chem simulated and observed relative contributions of different VOCs over Indian subcontinent.

**Table 3**  
WRF-Chem simulated mean  $\pm$  standard deviation values of major VOCs over different sub-regions in the Indian subcontinent during January 2011. The Percentage contributions of different VOCs to the total VOC simulated for different sub-regions are also given in parentheses.

VOCs (ppbv)	IGP	NER	CI	WI	SI	BoB	AS
Ethane	6.9 $\pm$ 4.2 (24.8)	5.3 $\pm$ 3.9 (19.1)	3.6 $\pm$ 0.44 (12.9)	4.5 $\pm$ 1.21 (16.2)	2.9 $\pm$ 0.86 (10.4)	2.6 $\pm$ 0.43 (9.3)	2 $\pm$ 0.56 (7.2)
Ethene	8.3 $\pm$ 6.8 (36.3)	4.4 $\pm$ 4.0 (19.3)	3.9 $\pm$ 0.64 (17.1)	3.4 $\pm$ 1.73 (14.8)	2.02 $\pm$ 2 (8.8)	0.73 $\pm$ 0.09 (3.2)	0.1 $\pm$ 0.10 (0.43)
Propane	16 $\pm$ 11.8 (32.1)	9.1 $\pm$ 7.4 (18.3)	8.2 $\pm$ 0.96 (16.5)	8 $\pm$ 3.25 (16.1)	4.6 $\pm$ 3.0 (9.3)	2.5 $\pm$ 0.58 (5)	1.3 $\pm$ 0.9 (2.6)
Propene	1.5 $\pm$ 1.1 (32.1)	1 $\pm$ 0.8 (21.4)	0.9 $\pm$ 0.18 (19.3)	0.58 $\pm$ 0.39 (12.4)	0.53 $\pm$ 0.6 (11.3)	0.16 $\pm$ 0.10 (3.4)	0.0003 $\pm$ 0.002 (0.01)
Pentane	5.1 $\pm$ 5.5 (36.23)	2 $\pm$ 1.7 (14.2)	2.1 $\pm$ 0.56 (14.9)	2.7 $\pm$ 1.35 (19.1)	1.3 $\pm$ 1.0 (9.2)	0.6 $\pm$ 0.20 (4.2)	0.27 $\pm$ 0.26 (1.9)
Acetaldehyde	5.3 $\pm$ 3.6 (25.3)	4 $\pm$ 2.7 (19.1)	4.5 $\pm$ 1.21 (21.5)	3.2 $\pm$ 1.41 (15.3)	2.3 $\pm$ 2.2 (11)	1.2 $\pm$ 0.36 (5.7)	0.37 $\pm$ 0.27 (1.8)
Acetone	4.3 $\pm$ 2.5 (20.4)	3.4 $\pm$ 2.1 (16.1)	3 $\pm$ 0.28 (14.3)	3.3 $\pm$ 0.80 (15.7)	2.5 $\pm$ 0.8 (11.9)	2.4 $\pm$ 0.43 (11.4)	2.1 $\pm$ 0.72 (10)
Toluene	3.2 $\pm$ 2.6 (36.6)	1.8 $\pm$ 1.6 (20.6)	1.2 $\pm$ 0.24 (13.7)	1.4 $\pm$ 0.69 (16.1)	0.68 $\pm$ 0.6 (7.8)	0.36 $\pm$ 0.06 (4.1)	0.08 $\pm$ 0.10 (0.9)

by Mahajan et al. (2015) over Indian region. In CI, increasing industrialization, vehicular emissions and agricultural waste burning (Sarkar et al., 2015) contribute to the HCHO loading. Interestingly, WRF-Chem as well as MACC reanalysis reveal enhanced HCHO mixing ratios over the western coast of southern India ( $>3$  ppbv). Rapid oxidation of VOCs (also from large vegetation fraction) in the presence of elevated ozone is suggested as the major source of HCHO over the western coast. Similarly, oxidation of biogenic emissions in the thick vegetation covered regions can enhance the formation of HCHO over NER. These regional differences are further investigated by comparing the tropospheric

column HCHO dataset of WRF-Chem, MACC reanalysis and satellite-based observations.

Fig. 6 shows the spatial distribution of tropospheric columns of formaldehyde and glyoxal over the Indian subcontinent from the WRF-Chem simulation and satellite-based measurements from the OMI, GOME-2A and SCIAMACHY. The bias plots of HCHO and CHOCHO between WRF-Chem model and satellite-based measurements are shown in Fig. S3 (Supplementary material). Satellite retrievals of January from multi-year observations have been averaged to reduce the noise. Formaldehyde data available from the MACC reanalysis for January 2011 is also shown for a comparison.

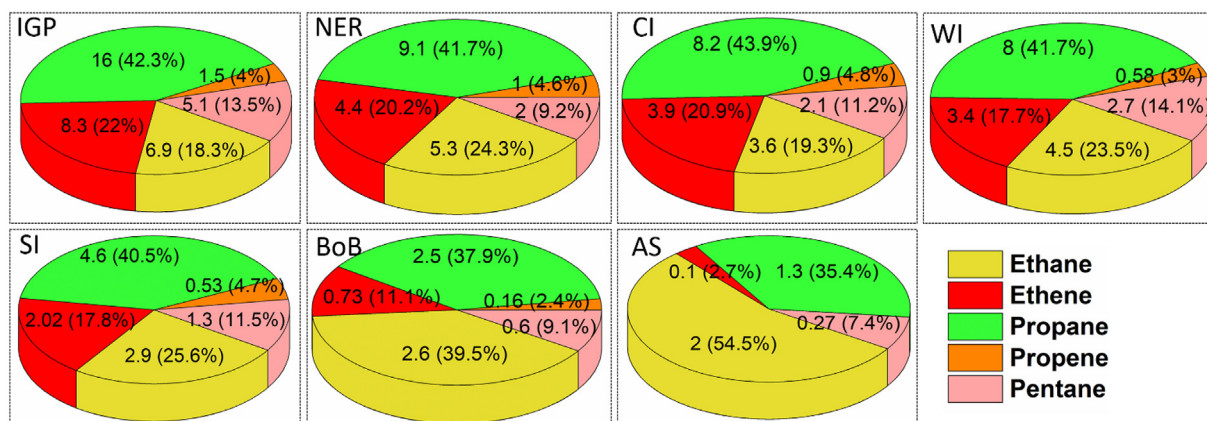


Fig. 4. Comparison of the relative abundances of different VOCs over different sub-regions of Indian subcontinent based on WRF-Chem.

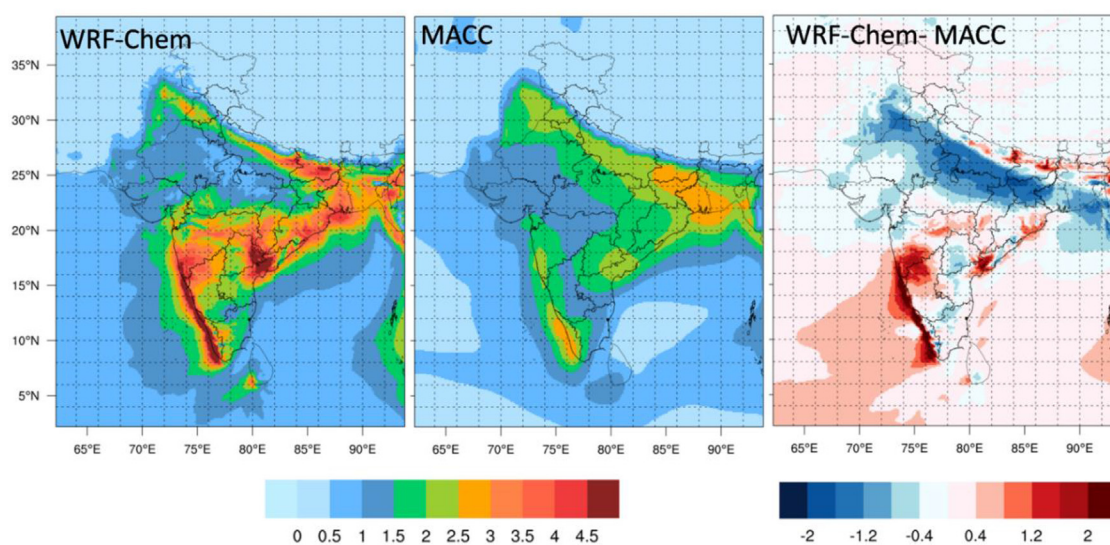


Fig. 5. Spatial distribution of near surface mixing ratios of HCHO from WRF-Chem, MACC reanalysis and the difference (ppbv) during January 2011.

Table 4

Near surface mean mixing ratios (ppbv) of HCHO from WRF-Chem and MACC reanalysis along with mean bias and correlation coefficient (r) over Indian subcontinent during January 2011.

Sub-region	HCHO from WRF-Chem	HCHO from MACC reanalysis	Mean Bias (MB)	Correlation coefficient (r)
IGP	1.4 ± 1.0	1.6 ± 0.79	−0.2	0.69
NER	1.8 ± 1.2	1.4 ± 0.96	0.4	0.88
CI	2.6 ± 0.72	1.6 ± 0.22	1	0.27
WI	1.7 ± 0.75	1.2 ± 0.33	0.5	0.81
SI	2.1 ± 1.2	1.3 ± 0.60	0.8	0.84
BoB	1.3 ± 0.36	0.95 ± 0.18	0.35	0.92
AS	0.94 ± 0.23	0.56 ± 0.14	0.38	0.94

WRF-Chem simulation of formaldehyde show elevated loadings of  $6\text{--}14 \times 10^{15}$  molecules  $\text{cm}^{-2}$  over the IGP, NER, and western coast, in agreement with those of satellite-based observations and the MACC reanalysis. However, significant differences can be noticed among retrievals from different satellite-based instruments, in particular over CI, where OMI (in agreement with WRF-Chem) shows higher ( $10\text{--}12 \times 10^{15}$  molecules  $\text{cm}^{-2}$ ) HCHO loadings, but such enhancements are not observed in the GOME-2A and SCIAMACHY. MACC HCHO shows a good agreement (percentage difference less than 20%) with SCIAMACHY data which is

consistent with previous results by Inness et al. (2013). Spatial distribution of glyoxal is simulated to be similar to formaldehyde with enhanced levels over the IGP, NER and western coast of the southern India. Satellite-based observations also show higher glyoxal levels over the IGP, nevertheless modeled values are significantly higher than the observations (Supplementary material, Fig. S3). WRF-Chem generally overestimates the satellite retrievals over the Indian landmass with mean bias ranging from  $0.03 \times 10^{14}$  to  $4 \times 10^{14}$  molecule  $\text{cm}^{-2}$ , whereas model underestimates over the oceanic region. Correlated HCHO–CHOCHO

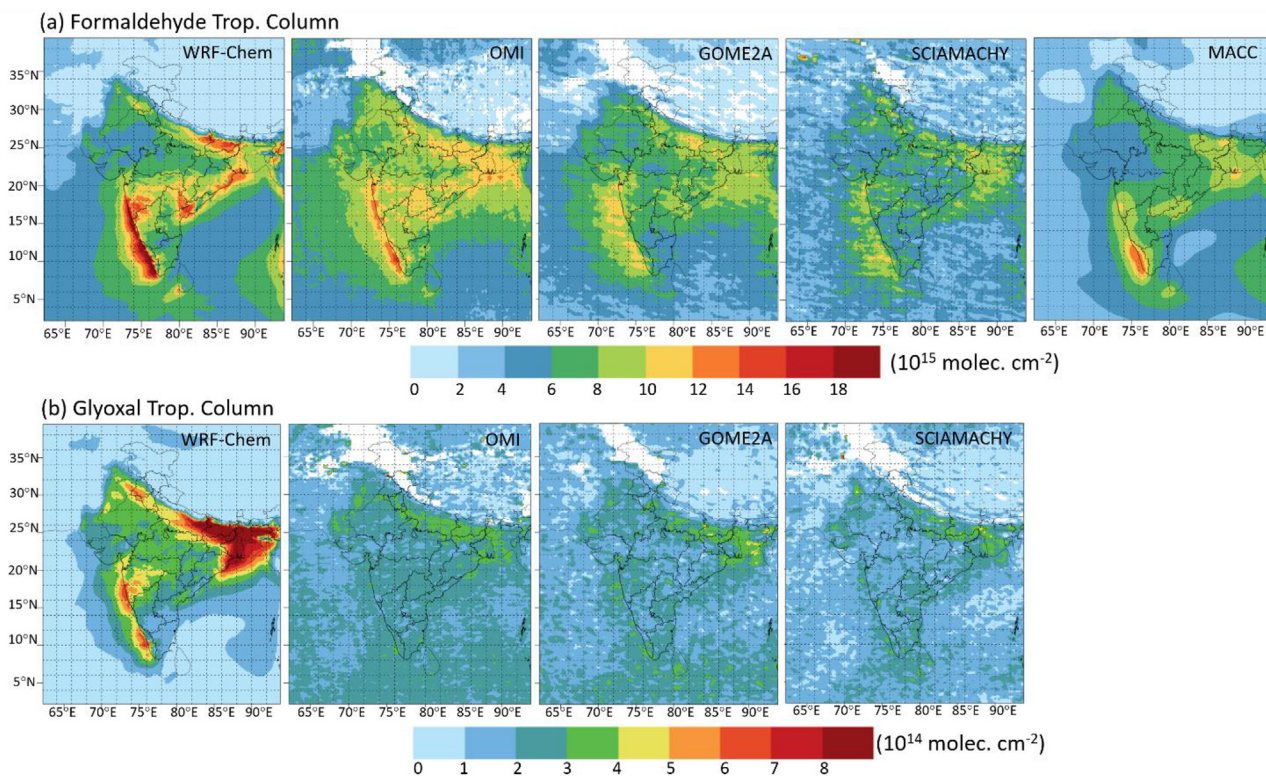


**Fig. 6.** Spatial distribution of tropospheric column (a) HCHO and (b) CHOCHO from WRF-Chem, MACC reanalysis, OMI, GOME-2A and SCIAMACHY over Indian subcontinent.

distributions (Supplementary Material-Table S4) over NER and IGP ( $r > 0.56$ ) reflect the role of their similar regional emissions and photochemistry across these sub-regions, unlike CI ( $r < 0.2$ ) where transport seems to play an important role.

OMI-retrieved HCHO and CHOCHO tropospheric columns are comparatively higher than GOME2A and SCIAMACHY retrieved column over Indian subcontinent by 5–33%. The disagreements could be due to the differences in resolution and sampling of different air masses due to difference in overpass times. Higher loadings of HCHO and CHOCHO by OMI in comparison to GOME2A and SCIAMACHY over the land have been reported in few studies earlier (e.g. De Smedt et al., 2015; De Smedt et al., 2010). OMI retrieved CHOCHO is shown to be in good agreement with GOME-2 and SCIAMACHY observations over regions of larger biogenic emissions, whereas, differences are more pronounced over the areas of strong anthropogenic and biomass-burning emissions (Alvarado et al., 2014). This is corroborated with the distribution of Normalized Difference Vegetation Index (NDVI) obtained from MODIS over Indian subcontinent by identifying the regions of biogenic emissions (Supplementary material, Fig. S4). Higher vegetation index over NER and SI plays a dominant role in the formation of HCHO and CHOCHO from the oxidation of biogenic precursors over these two sub-regions. In contrast, a poor correlation between the NDVI and HCHO (CHOCHO) is observed over IGP indicating biogenic emissions can be less significant over this region. Tropospheric column of  $\text{NO}_2$  can be used as a tracer to estimate the influence of anthropogenic emissions. Enhanced column loadings of HCHO, CHOCHO and  $\text{NO}_2$  over IGP are attributed to the strong anthropogenic emissions during winter (Supplementary material, Fig. S5).

We further use the ratio of tropospheric CHOCHO to HCHO (CHOCHO/HCHO), denoted by  $R_{GF}$ , as a tracer of dominant VOC sources (see e.g. Vrekoussis et al., 2010 and references therein).

Earlier studies have reported  $R_{GF}$  values in the range of 0.04–0.06 over the regions of biogenic emissions, while, lower  $R_{GF}$  values were observed in polluted urban environments. Spatial distribution of  $R_{GF}$  over Indian subcontinent from the WRF-Chem simulation and satellite-based measurements from the OMI, GOME2A and SCIAMACHY is shown in Fig. 7.

$R_{GF}$ , based on the model results and satellite retrievals, is found to vary in the range of 0.0–0.07 over Indian subcontinent. WRF-Chem estimated  $R_{GF}$  is lower than 0.04 over all sub-regions, except NER and WI ( $R_{GF} = 0.042$  at WI,  $R_{GF} = 0.069$  at NER). Strong  $\text{NO}_x$  emission over the IGP intensify the tropospheric chemistry and enhance HCHO (Wolfe et al., 2016), resulting in lower  $R_{GF}$  over this region. Hoque et al. (2018) reported  $R_{GF} = 0.03$  over IGP indicating influences of biomass burning and anthropogenic emission over IGP. The vegetation cover over some parts of NER could have contributed to the higher  $R_{GF}$  confirming significant biogenic effects, in addition to anthropogenic emissions over Bangladesh region. Satellite-based observations show similar spatial distributions with  $R_{GF}$  levels lower than 0.04 over different sub-regions. WRF-Chem overestimates the OMI, GOME2A and SCIAMACHY retrieved  $R_{GF}$  by 34–53% over WI and NER.  $R_{GF}$  values derived from WRF-Chem and satellite-based measurements reveal that VOCs from the anthropogenic sources are the major contributor over sub-regions of Indian subcontinent, except over NER. Higher  $R_{GF}$  value ( $R_{GF} > 0.04$ ) over NER is partially due to the biogenic emissions, besides anthropogenic emissions contributing to this region. To further corroborate these findings, it is highly desirable to initiate the in-situ observations over this region in near future.

#### 4.3. Ozone formation regimes: WRF-Chem versus satellite data

In this section, we use the WRF-Chem set up, evaluated for VOCs in previous sections, to compute the  $[\text{HCHO}]/[\text{NO}_y]$  ratio and

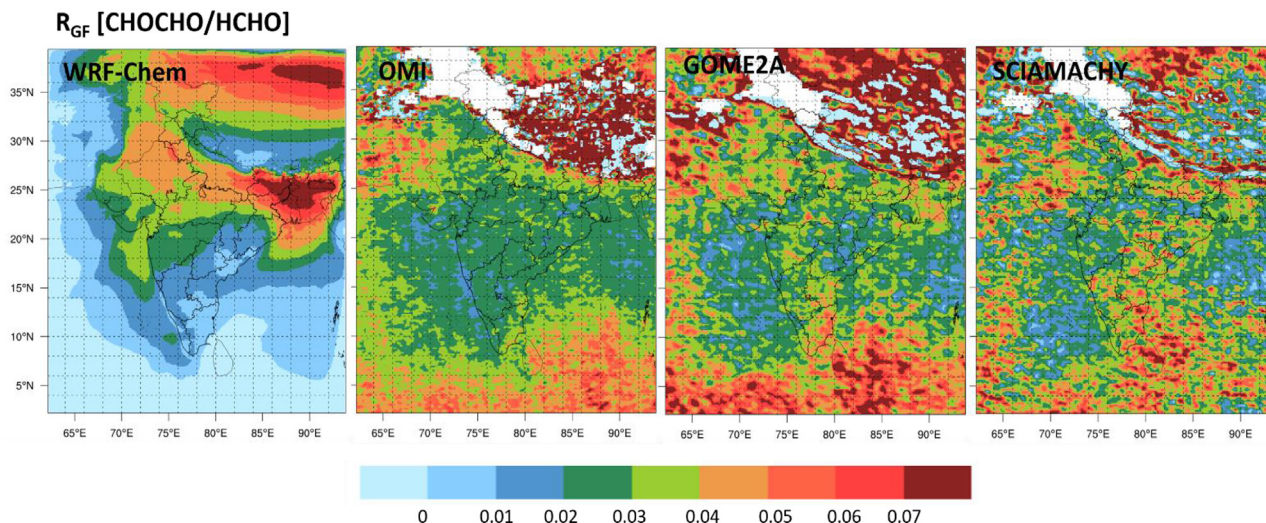


Fig. 7. Spatial distributions of  $R_{GF}$  obtained from WRF-Chem, OMI, GOME-2A, and SCIAMACHY over Indian subcontinent.

compare the model results with OMI observations. As the production of HCHO is proportional to reactions of reactive organics with OH radical, lower values of  $[HCHO]/[NO_y]$  are associated with VOC-limited chemical environments (Sillman, 1995). Sillman (1995) considered value of 0.28 for the  $[HCHO]/[NO_y]$  ratio as a transitional value from VOC-limited to  $NO_x$ -limited regime, which has been applied successfully in various studies (Kumar et al., 2012b).

Model simulated average noontime (11:30–14:30 IST) surface  $[HCHO]/[NO_y]$  as well as tropospheric  $[HCHO]/[NO_2]$  ratios are computed. Fig. 8 show the spatial distribution of WRF-Chem simulated average noontime (11:30–14:30 IST) surface  $[HCHO]/[NO_y]$  ratio during January 2011. The  $[HCHO]/[NO_y]$  ratio is lower than 0.28 over western part of IGP and eastern part of CI, indicating VOC-limited ozone chemistry. The  $[HCHO]/[NO_y]$  ratio is seen to be greater than 0.28 over the other regions of India indicating prevalence of  $NO_x$ -limited ozone chemistry. Further studies based on in situ measurements of VOCs and  $NO_x$  need to be carried out for further insight.

To evaluate this model-based result, noontime tropospheric column  $[HCHO]/[NO_2]$  ratios are also estimated from space-based observations. Duncan et al. (2010) have considered  $[HCHO]/[NO_2]$  ratios  $>2.0$  as an indicator of  $NO_x$ -limited) and ratios  $<1.0$  as VOC-limited ozone production. The ratios between 1 and 2 represent the transition regime where the formation of ozone becomes sensitive to both  $NO_x$  and VOC. Fig. 9 shows the spatial distributions of tropospheric columnar HCHO/ $NO_2$  ratio obtained from WRF-Chem and OMI over Indian subcontinent. Similar to the surface  $[HCHO]/[NO_y]$  ratio, WRF-Chem simulated tropospheric HCHO/ $NO_2$  ratio shows the VOC-limited chemistry over western part of IGP and eastern part of CI. However, OMI retrieved tropospheric ratios show that these regions fall under the transition regime where both  $NO_x$  and VOC are important.

Apart from IGP and CI, all other regions represents  $NO_x$  limited regime further indicating that reductions of  $NO_x$  limited ozone chemistry. Ratios are found to be slightly higher in estimation based on OMI observations compared to the model over all the regions; however, both WRF-Chem and OMI analysis show similar spatial distribution confirming the dominance of  $NO_x$  limited ozone production over most parts of the Indian region. Nevertheless, the production of ozone over the IGP and CI may respond to the changes in VOCs emissions, besides  $NO_x$ .

## 5. Summary and conclusions

In this study, the distribution of VOCs over Indian subcontinent has been analyzed by combining a regional model WRF-Chem with observations and reanalysis data during winter season. Model

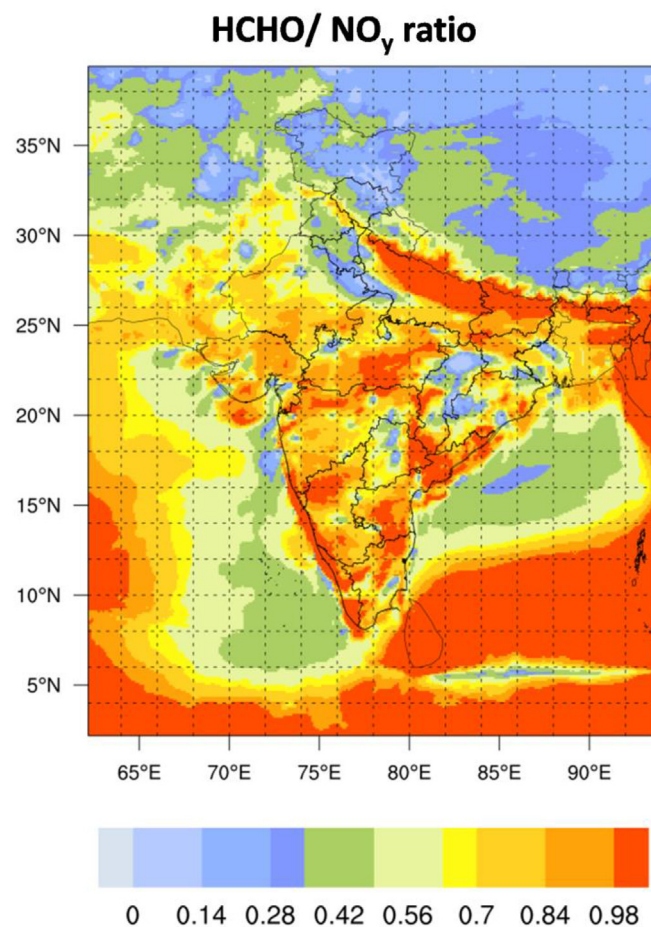


Fig. 8. Spatial distribution of WRF-Chem simulated average noontime (11:30–14:30 IST) surface ratio of  $[HCHO]/[NO_y]$  over the Indian subcontinent for January 2011.

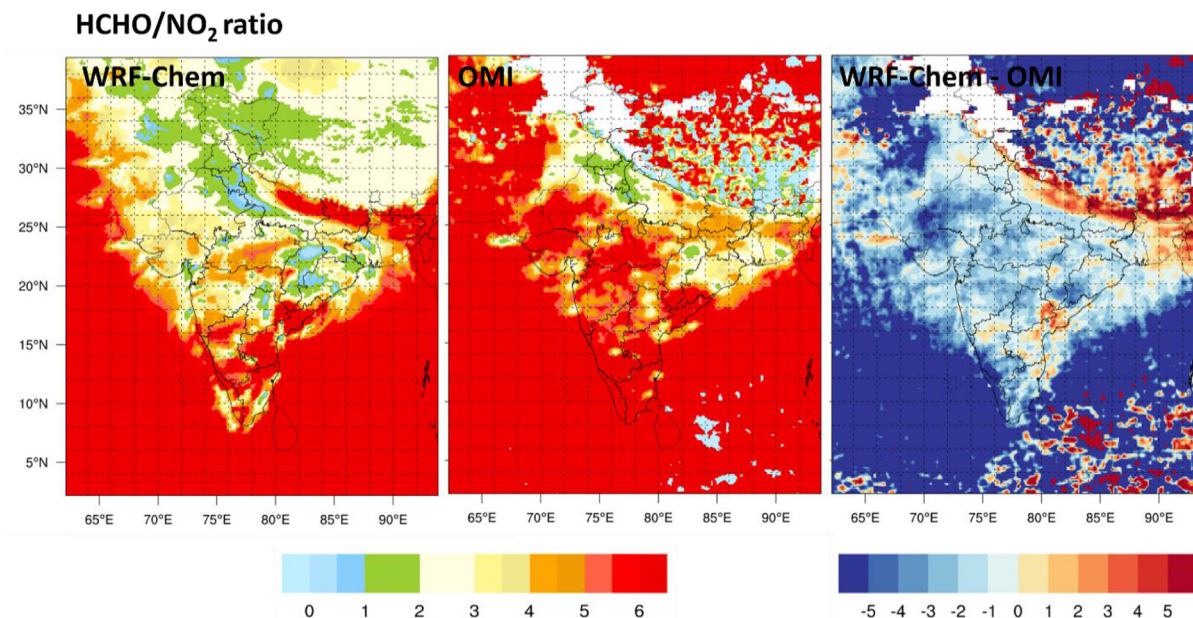


Fig. 9. Spatial distribution of tropospheric columnar ratio of HCHO/NO<sub>2</sub> obtained from (a) WRF-Chem (b) OMI (c) WRF-Chem-OMI over Indian subcontinent.

results reveal strong spatial heterogeneity in the distribution of VOCs with higher levels over the IGP and NER regions. Among the measured VOCs, propane and ethane show dominant contributions, compared to more reactive species ethene and propene, due to their longer lifetime and better mixing. Modeled glyoxal columns are maximum over IGP and NER, in agreement with strong anthropogenic emissions and higher vegetation index indicating intense photochemistry. Spatial distributions of HCHO and CHOCHO obtained from OMI, GOME2A and SCIAMACHY are similar, however OMI retrieved column values are higher than GOME2A and SCIAMACHY. Better HCHO–CHOCHO correlations over NER and IGP point to common sources in these regions.  $R_{GF}$  derived from model and satellite-based observations reveal that VOC loadings are predominantly from the anthropogenic sources over all sub regions in the Indian subcontinent, except at NER. Higher  $R_{GF}$  value ( $\sim 0.069$ ) over NER is associated with the significant vegetation fraction leading to biogenic emissions, besides the anthropogenic emissions over the region. The  $[HCHO]/[NO_2]$  ratios for surface (WRF-Chem simulation) and tropospheric column (OMI observations) show that ozone formation is NO<sub>x</sub> limited over India. Higher concentrations of primary VOCs along with elevated levels of HCHO and CHOCHO over IGP and NER indicate stronger emissions and photochemical processing and have important implication for regional tropospheric chemistry including the formation of ozone and secondary organic aerosols and climate.

The present study provides a comparison of model results, observations (in situ and satellites) and chemical reanalysis for a first-hand information on the distribution of VOCs across the Indian subcontinent. The improvements in model set up as well as inputs are important to consider in future studies. Considering significant differences not only between model and observations, but also among the retrievals from different satellite-based instruments, our study highlights a need of in situ observational network for VOCs across the South Asia. Observations are especially required over the identified regional hotspots (NER, central India, and the western coast) based on model results. VOC emissions over Indian region shows an increasing trend based on MACCity anthropogenic emissions data. Long-term systematic observations together with development of time varying emission inventories are highly

desirable for a detailed assessment of VOCs trends over different sub-regions. Moreover, development of VOC speciation of anthropogenic emissions, specific to Indian region, is needed to improve the model results in reproducing the relative abundances to better understand the tropospheric chemistry of the VOCs and its implications in South Asia and downwind.

### Acknowledgements

LC acknowledges the DST-INSPIRE fellowship program, Govt. of India for providing financial support to undertake this work. Era interim dataset used as the initial and boundary condition for meteorological fields to the WRF is acknowledged. We acknowledge use of the WRF-Chem preprocessor tools (anthro\_emis, bio\_emiss, fire\_emiss, mozbc etc.) provided by the Atmospheric Chemistry Observations and Modeling Lab (ACOM) of NCAR. We acknowledge use of NCAR/ACOM MOZART-4 global model output available at <http://www.acom.ucar.edu/wrf-chem/mozart.shtml>. The HTAP v2 anthropogenic emissions were obtained from [http://edgar.jrc.ec.europa.eu/htap\\_v2/index.php?SECURE=123](http://edgar.jrc.ec.europa.eu/htap_v2/index.php?SECURE=123). Biomass burning emissions were obtained from the NCAR Fire Inventory (<http://bai.acom.ucar.edu/Data/fire/>). Use of MACC reanalysis data (<http://apps.ecmwf.int/datasets/data/macc-reanalysis/>) is acknowledged. Tropospheric H<sub>2</sub>CO columns are derived at BIRA from GOME2A and OMI observations using DOAS technique were obtained from <http://h2co.aeronomie.be/>. Tropospheric glyoxal data from OMI and GOME2A were downloaded from [http://www.iup.uni-bremen.de/does/glyoxal\\_data.htm](http://www.iup.uni-bremen.de/does/glyoxal_data.htm) are gratefully acknowledged. The Dutch-Finnish-built OMI is part of the NASA EOS Aura satellite payload. The OMI project is managed by NIVR and KNMI in Netherlands. The tropospheric NO<sub>x</sub> data were obtained from [https://acd-disc.gesdisc.eosdis.nasa.gov/data/Aura\\_OMI\\_Level3/](https://acd-disc.gesdisc.eosdis.nasa.gov/data/Aura_OMI_Level3/). The contributions of the University of Bremen scientists to this manuscript are funded in part by the University and State of Bremen, DLR (German Aerospace), DFG and ES. The authors acknowledge the use of Vikram-HPC at PRL, Ahmedabad for model simulations. The authors thank three anonymous reviewers for their constructive comments and valuable suggestions.

## Appendix A. Supplementary data

Supplementary data to this article can be found online at <https://doi.org/10.1016/j.envpol.2019.05.097>.

## References

- Ackermann, I.J., Hass, H., Memmesheimer, M., Ebel, A., Binkowski, F.S., Shankar, U., 1998. Modal aerosol dynamics model for Europe: development and first applications. *Atmos. Environ.* 32 (17), 2981–2999. [https://doi.org/10.1016/S1352-2310\(98\)00006-5](https://doi.org/10.1016/S1352-2310(98)00006-5).
- Akimoto, H., Ohara, T., Kurokawa, J., Horii, N., 2006. Verification of energy consumption in China during 1996–2003 by using satellite observational data. *Atmos. Environ.* 40, 7663–7667. <https://doi.org/10.1016/j.atmosenv.2006.07.052>.
- Alvarado, L.M.A., Richter, A., Vrekoussis, M., Wittrock, F., Hilboll, A., Schreier, S.F., Burrows, J.P., 2014. An improved glyoxal retrieval from OMI measurements. *Atmos. Meas. Tech.* 7, 4133–4150. <https://doi.org/10.5194/amt-7-4133-2014>.
- Arlander, D.W., Bruning, D., Schmidt, U., Ehhalt, D.H., 1995. The tropospheric distribution of formaldehyde during TROPOZ II. *J. Atmos. Chem.* 22 (3), 251–268.
- Atkinson, R., 2000. Atmospheric chemistry of VOCs and NOx. *Atmos. Environ.* 34 (12–14), 2063–2101. [https://doi.org/10.1016/S1352-2310\(99\)00460-4](https://doi.org/10.1016/S1352-2310(99)00460-4).
- Bhardwaj, P., Naja, M., Rupakheti, M., Lupascu, A., Mues, A., Panday, A.K., Kumar, R., Mahata, K. s., Lal, S., Chandola, H.C., Lawrence, M.G., 2018. Variations in surface ozone and carbon monoxide in the Kathmandu Valley and surrounding broader regions during SusKat-ABC field campaign: role of local and regional sources. *Atmos. Chem. Phys.* 18, 11949–11971. <https://doi.org/10.5194/acp-18-11949-2018>.
- Burrows, J.P., Hölzle, E., Goede, A.P.H., Visser, H., Fricke, W., 1995. SCIAMACHY – scanning imaging absorption spectrometer for atmospheric chartography. *Acta Astronaut.* 35 (7), 445–451. [https://doi.org/10.1016/0094-5765\(94\)00278-T](https://doi.org/10.1016/0094-5765(94)00278-T).
- Callies, J., Corpaccioli, E., Eisinger, M., Hahne, A., Lefebvre, A., 2000. GOME-2 – metop's second-generation sensor for operational ozone monitoring. *ESA Bull. Eur. Space* 102, 28–36.
- Census of India, 2011. *Population Totals. Rural-Urban Distribution, Govt of India. Paper 2, Volume 1 of 2011*.
- Chang, C.Y., Faust, E., Hou, X., Lee, P., Kim, H.C., Hedquist, B.C., Liao, K.J., 2016. Investigating ambient ozone formation regimes in neighboring cities of shale plays in the Northeast United States using photochemical modeling and satellite retrievals. *Atmos. Environ.* 142, 152–170. <https://doi.org/10.1016/j.atmosenv.2016.06.058>.
- Chen, F., Dudhia, J., 2001. Coupling an advanced land surface-hydrology model with the Penn State-NCAR MM5 modeling system. Part I. Model implementation and sensitivity. *Mon. Weather Rev.* 129, 569–585. [https://doi.org/10.1175/1520-0493\(2001\)129<0569:CAALSH>2.0.CO;2](https://doi.org/10.1175/1520-0493(2001)129<0569:CAALSH>2.0.CO;2).
- Chou, M.D., Suarez, M.J., 1994. An efficient thermal infrared radiation parameterization for use in general circulation models. NASA Tech. Memorandum 104606 3, 85 (NASA, GoddardSpace Flight Center, Greenbelt, Maryland).
- De Smedt, I., Stavrou, T., Hendrick, F., Danckaert, T., Vlemmix, T., Pinardi, G., Heyes, N., Lerot, C., Gielen, C., Vigouroux, C., Hermans, C., Fayt, C., Veeckind, P., Müller, J.F., Van Roozendaal, M., 2015. Diurnal, seasonal and long-term variations of global formaldehyde columns inferred from combined OMI and GOME-2 observations. *Atmos. Chem. Phys.* 15, 12519–12545. <https://doi.org/10.5194/acp-15-12519-2015>.
- De Smedt, I., Stavrou, T., Müller, J.F., Van Der A, R.J., Van Roozendaal, M., 2010. Trend detection in satellite observations of formaldehyde tropospheric columns. *Geophys. Res. Lett.* 37, L18808. <https://doi.org/10.1029/2010GL044245>.
- De Smedt, I., Müller, J.-F., Stavrou, T., Van Der A, R., Eskes, H., Van Roozendaal, M., 2008. Twelve years of global observations of formaldehyde in the troposphere using GOME and SCIAMACHY sensors. *Atmos. Chem. Phys.* 8, 4947–4963. <https://doi.org/10.5194/acp-8-4947-2008>.
- Dixon, J.L., Beale, R., Nightingale, P.D., 2013. Production of methanol, acetaldehyde and acetone in the Atlantic Ocean. *Geophys. Res. Lett.* 40, 4700–4705. <https://doi.org/10.1002/grl.50922>.
- Duncan, B.N., Yoshida, Y., Olson, J.R., Sillman, S., Martin, R.V., Lamsal, L., Hu, Y.T., Pickering, K.E., Retscher, C., Allen, D.J., Crawford, J.H., 2010. Application of OMI observations to a space-based indicator of NOx and VOC controls on surface ozone formation. *Atmos. Environ.* 44 (18), 2213–2223. <https://doi.org/10.1016/j.atmosenv.2010.03.010>.
- Emmons, L.K., Walters, S., Hess, P.G., Lamarque, J.F., Pfister, G.G., Fillmore, D., Granier, C., Guenther, A., Kinnison, D., Laepple, T., Orlando, J., Tie, X., Tyndall, G., Wiedinmyer, C., Baughcum, S.L., Kloster, S., 2010. Description and evaluation of the model for ozone and related chemical tracers, version 4 (MOZART-4). *Geosci. Model Dev.* 3, 43–67. <https://doi.org/10.5194/gmd-3-43-2010>.
- Filley, C.M., Halliday, W., Kleinschmidt-Demasters, B.K., 2004. The effects of toluene on the central nervous system. *J. Neuropathol. Exp. Neurol.* 63 (1), 1–12.
- Fischer, E.V., Jacob, D.J., Millet, D.B., Yantosca, R.M., Mao, J., 2012. The role of the ocean in the global atmospheric budget of acetone. *Geophys. Res. Lett.* 39. <https://doi.org/10.1029/2011GL050086>.
- Fu, X., Wang, S.X., Zhao, B., Xing, J., Cheng, Z., Liu, H., Hao, J.M., 2013. Emission inventory of primary pollutants and chemical speciation in 2010 for the Yangtze River Delta region, China. *Atmos. Environ.* 70, 39–50.
- Fu, T.M., Jacob, D.J., Wittrock, F., Burrows, J.P., Vrekoussis, M., Henze, D.K., 2008. Global budgets of atmospheric glyoxal and methyl glyoxal, and implications for formation of secondary organic aerosols. *J. Geophys. Res. Atmos.* 113, D15303. <https://doi.org/10.1029/2007JD009505>.
- Fu, T.M., Jacob, D.J., Palmer, P.L., Chance, K., Wang, Y.X., Barletta, B., Blake, D.R., Stanton, J.C., Pilling, M.J., 2007. Space-based formaldehyde measurements as constraints on volatile organic compound emissions in east and South Asia and implications for ozone. *J. Geophys. Res.* 112 (D6). <https://doi.org/10.1029/2006JD007853>.
- Girach, I.A., Ojha, N., Nair, P.R., Pozzer, A., Tiwari, Y.K., Kumar, K.R., Lelieveld, J., 2017. Variations in O3, CO, and CH4 over the Bay of Bengal during the summer monsoon season: shipborne measurements and model simulations. *Atmos. Chem. Phys.* 17, 257–275. <https://doi.org/10.5194/acp-17-257-2017>.
- Glass, D.C., Gray, C.N., Jolley, D.J., Gibbons, C., Sim, M.R., Fritsch, L., Adams, G.G., Bisby, J.A., Manuell, R., 2003. Leukemia risk associated with low-level benzene exposure. *Epidemiology* 14 (5), 569–577. <https://doi.org/10.1097/01.ede.0000082001.05563.e0>.
- Gogoi, M.M., Babu, S.S., Moorthy, K.K., Bhuyan, P.K., Pathak, B., Subba, T., Chutia, L., Kundu, S.S., Bharali, C., Borgohain, A., Guha, A., De, B.K., Singh, B., Chin, M., 2017. Radiative effects of absorbing aerosols over Northeastern India: observations and model simulations. *J. Geophys. Res. Atmos.* 122, 1132–1157. <https://doi.org/10.1002/2016JD025592>.
- Grell, G.A., Peckham, S.E., Schmitz, R., McKeen, S.A., Frost, G., Skamarock, W.C., Eder, B., 2005. Fully coupled 'online' chemistry within the WRF model. *Atmos. Environ.* 39, 6957–6975. <https://doi.org/10.1016/j.atmosenv.2005.04.027>.
- Grell, G.A., Devenyi, D., 2002. A generalized approach to parameterizing convection combining ensemble and data assimilation techniques. *Geophys. Res. Lett.* 29, 38–41. <https://doi.org/10.1029/2002GL015311>.
- Grell, G., 1993. Prognostic evaluation of assumptions used by cumulus parameterizations. *Mon. Weather Rev.* 121, 764–787. [https://doi.org/10.1175/1520-0493\(1993\)121<0764:PEOAU>2.0.CO;2](https://doi.org/10.1175/1520-0493(1993)121<0764:PEOAU>2.0.CO;2).
- Guenther, A.B., Jiang, X., Heald, C.L., Sakulyanontvittaya, T., Duhl, T., Emmons, L.K., Wang, X., 2012. The Model of Emissions of Gases and Aerosols from Nature version 2.1 (MEGAN2.1): an extended and updated framework for modeling biogenic emissions. *Geosci. Model Dev.* 5, 1471–1492. <https://doi.org/10.5194/gmd-5-1471-2012>.
- Guenther, A.B., Karl, T., Harley, P., Wiedinmyer, C., Palmer, P.I., Geron, C., 2006. Estimates of global terrestrial isoprene emissions using MEGAN (model of emissions of gases and aerosols from nature). *Atmos. Chem. Phys.* 6, 3181–3210. <https://doi.org/10.5194/acp-6-3181-2006>.
- Guo, H., Lee, S.C., Chan, L.Y., Li, W.M., 2004. Risk assessment of exposure to volatile organic compounds in different indoor environments. *Atmos. Res.* 94, 57–66.
- Hoque, H.M.S., Irie, H., Damiani, A., Rawat, P., Naja, M., 2018. First simultaneous observations of formaldehyde and glyoxal by MAX-DOAS in the Indo-Gangetic Plain region. *SOLA* 14, 159–164. <https://doi.org/10.2151/sola.2018-028>.
- Huang, G., Brook, R., Crippa, M., Janssens-Maenhout, G., Schieberle, C., Dore, C., Guizzardi, D., Muntean, M., Schaaf, E., Friedrich, R., 2017. Speciation of anthropogenic emissions of non-methane volatile organic compounds: a global gridded data set for 1970–2012. *Atmos. Chem. Phys.* 17, 7683–7701. <https://doi.org/10.5194/acp-17-7683-2017>.
- Inness, A., Baier, F., Benedetti, A., Bouarar, I., Chabrillat, S., Clark, H., Clerbaux, C., Coheur, P., Engelen, R.J., Errera, Q., Flemming, J., George, M., Granier, C., Hadji-Lazarou, J., Huijnen, V., Hurtmans, D., Jones, L., Kaiser, J.W., Kapsomenakis, J., Lefever, K., Leifao, J., Razinger, M., Richter, A., Schultz, M.G., Simmons, A.J., Suttie, M., Stein, O., Thépaut, J.N., Thouret, V., Vrekoussis, M., Zerefos, C., The MACC team, 2013. The MACC reanalysis: an 8 yr data set of atmospheric composition. *Atmos. Chem. Phys.* 13, 4073–4109. <https://doi.org/10.5194/acp-13-4073-2013>.
- Janjić, Z.I., 2002. Nonsingular implementation of the Mellor–Yamada Level 2.5 scheme in the NCEP meso model. *NCEP Off. Note* 437, 61.
- Janjić, Z.I., 1996. The surface layer in the NCEP Eta Model. In: *Eleventh Conference on Numerical Weather Prediction, Norfolk, VA, 19–23 August, Am. Meteor. Soc., Boston, MA*, pp. 354–355.
- Janssens-Maenhout, G., Crippa, M., Guizzardi, D., Dentener, F., Muntean, M., Pouliot, G., Keating, T., Zhang, Q., Kurokawa, J., Wankmüller, R., Denier Van Der Gon, H., Kuenen, J.J.P., Klimont, Z., Frost, G., Darras, S., Koffi, B., Li, M., 2015. HTAP\_v2.2: a mosaic of regional and global emission grid maps for 2008 and 2010 to study hemispheric transport of air pollution. *Atmos. Chem. Phys.* 15, 11411–11432. <https://doi.org/10.5194/acp-15-11411-2015>.
- Kandiyala, R., Raghavendra, S.P.C., Rajasekharan, S.T., 2010. Xylene: an overview of its health hazards and preventive measures. *J. Oral Maxillofac. Pathol.* 14 (1), 1–5.
- Kumar, D.B., Verma, S., 2016. Potential emission flux to aerosol pollutants over Bengal Gangetic plain through combined trajectory clustering and aerosol source fields analysis. *Atmos. Res.* 178–179, 415–425. <https://doi.org/10.1016/j.atmosres.2016.04.012>.
- Kumar, R., Naja, M., Pfister, G.G., Barth, M.C., Wiedinmyer, C., Brasseur, G.P., 2012b. Simulations over South Asia using the weather research and forecasting model with chemistry (WRF-Chem): chemistry evaluation and initial results. *Geosci. Model Dev.* 5, 619–648. <https://doi.org/10.5194/gmd-5-619-2012>.
- Kumar, R., Naja, M., Pfister, G.G., Barth, M.C., Brasseur, G.P., 2012a. Simulations over South Asia using the weather research and forecasting model with chemistry (WRF-Chem): set-up and meteorological evaluation. *Geosci. Model Dev.* 5, 321–343. <https://doi.org/10.5194/gmd-5-321-2012>.
- Laban, T.L., Zyl, P.G.V., Beukes, J.P., Vakkari, V., Jaars, K., Borduas-Dedekind, N., Josipovic, M., Thompson, A.M., Kulmal, M., Laakso, L., 2018. Seasonal influences on surface ozone variability in continental South Africa and implications for air

- quality. *Atmos. Chem. Phys.* 18, 15491–15514. <https://doi.org/10.5194/acp-18-15491-2018>.
- Lal, S., Sahu, L.K., Venkataramani, S., Mallik, C., 2012. Light non-methane hydrocarbons at two sites in the Indo-Gangetic Plain. *J. Environ. Monit.* 14 (4), 1159–1166. <https://doi.org/10.1039/c2em10682e>.
- Lawrence, M.G., Lelieveld, J., 2010. Atmospheric pollutant outflow from southern Asia: a review. *Atmos. Chem. Phys.* 10 <https://doi.org/10.5194/acp-10-11017-2010>, 11017–11096.
- Lee, Y.N., Zhou, X., Kleinman, L.I., Nunnermacker, L.J., Springston, S.R., Daum, P.H., Newman, L., Keigley, W.G., Holdren, M.W., Spicer, C.W., Young, V., Fu, B., Parrish, D.D., Holloway, J., Williams, J., Roberts, J.M., Ryerson, T.B., Fehsenfeld, F.C., 1998. Atmospheric chemistry and distribution of formaldehyde and several multioxygenated carbonyl compounds during the 1995 Nashville middle Tennessee ozone study. *J. Geophys. Res. Atmos.* 103 (D17), 22449–22462. <https://doi.org/10.1029/98JD01251>.
- Levelt, P.F., van den Oord, G.H.J., Dobber, M.R., Malkki, A., Huib, V., de Vries, J., Stammes, P., Lundell, J.O.V., Saari, H., 2006. The ozone monitoring instrument. *IEEE Trans. Geosci. Remote Sens.* 44 (5), 1093–1101. <https://doi.org/10.1109/TGRS.2006.872333>.
- Li, M., Zhang, Q., Kurokawa, J.-I., Woo, J.-H., He, K., Lu, Z., Ohara, T., Song, Y., Streets, D.G., Carmichael, G.R., Cheng, Y., Hong, C., Huo, H., Jiang, X., Kang, S., Liu, F., Su, H., Zheng, B., 2017. MIX: a mosaic Asian anthropogenic emission inventory under the international collaboration framework of the MICS-Asia and HTAP. *Atmos. Chem. Phys.* 17, 935–963. <https://doi.org/10.5194/acp-17-935-2017>.
- Li, M., Zhang, Q., Streets, D.G., He, K.B., Cheng, Y.F., Emmons, L.K., Huo, H., Kang, S.C., Lu, Z., Shao, M., Su, H., Yu, X., Zhang, Y., 2014. Mapping Asian anthropogenic emissions of non-methane volatile organic compounds to multiple chemical mechanisms. *Atmos. Chem. Phys.* 14, 5617–5638. <https://doi.org/10.5194/acp-14-5617-2014>.
- Lin, Y.L., Farley, R.D., Orville, H.D., 1983. Bulk parameterization of the snow field in a cloud model. *J. Clim. Appl. Meteorol.* 22, 1065–1092.
- Lindinger, W., Hansel, A., Jordan, A., 1998. On-line monitoring of volatile organic compounds at pptv levels by means of proton-transfer-reaction mass spectrometry (PTR-MS) - medical applications, food control and environmental research. *Int. J. Mass Spectrom.* 173, 191–241. [https://doi.org/10.1016/S0168-1176\(97\)00281-4](https://doi.org/10.1016/S0168-1176(97)00281-4).
- Logan, J.A., Prather, M.J., Wofsy, S.C., McElroy, M.B., 1981. Tropospheric chemistry: a global perspective. *J. Geophys. Res.* 86, 7210–7254. <https://doi.org/10.1029/JC086iC08p07210>.
- Mahajan, A.S., Smedt, I.D., Biswas, M.S., Ghude, S., Fadnavis, S., Roy, C., van Roozendaal, M., 2015. Inter-annual variations in satellite observations of nitrogen dioxide and formaldehyde over India. *Atmos. Environ.* 116, 194–201. <https://doi.org/10.1016/j.atmosenv.2015.06.004>.
- Majumdar, D., Mukherjee, A.K., Sen, S., 2011. BTEX in ambient air of a Metropolitan City. *J. Environ. Protection* 2, 11–20. <https://doi.org/10.4236/jep.2011.21002>.
- Martin, R.V., Fiore, A.M., Van Donkelaar, A., 2004. Space-based diagnosis of surface ozone sensitivity to anthropogenic emissions. *Geophys. Res. Lett.* 31, L06120. <https://doi.org/10.1029/2004GL019416>.
- Mlawer, E.J., Taubman, S.J., Brown, P.D., Iacono, M.J., Clough, S.A., 1997. Radiative transfer for inhomogeneous atmospheres: RRTM, a validated correlated-k model for the longwave. *J. Geophys. Res. Atmos.* 102, 16663–16682. <https://doi.org/10.1029/97JD00237>.
- Moorthy, K.K., Babu, S.S., Satheesh, S.K., 2005. Aerosol characteristics and radiative impacts over the Arabian Sea during the inter-monsoon season: results from ARMEX field campaign. *J. Atmos. Sci.* 62, 192–206. <https://doi.org/10.1175/JAS-3378.1>.
- Müller, J.F., 1992. Geographical distribution and seasonal variation of surface emissions and deposition velocities of atmospheric trace gases. *J. Geophys. Res.* 97, 3787–3804. <https://doi.org/10.1029/91JD02757>.
- Munger, J.W., Jacob, D.J., Daube, B.C., Horowitz, L.W., Keene, W.C., Heikes, B.G., 1995. Formaldehyde, glyoxal, and methylglyoxal in air and cloudwater at a rural mountain site in central Virginia. *J. Geophys. Res. Atmos.* 100, 9325–9333. <https://doi.org/10.1029/95JD00508>.
- Munro, R., Eisinger, M., Anderson, C., Callies, J., Corpaolioli, E., Lang, R., Lefebvre, A., Livschitz, Y., Albinana, A.P., 2006. GOME-2 on MetOp. In: *Proc. Of the 2006 EUMETSAT Meteorological Satellite Conference*, Helsinki, Finland. 12–16 June 2006. EUMETSAT, p. 48.
- Nair, V.S., et al., 2007. Wintertime aerosol characteristics over the Indo-Gangetic Plain (IGP): impacts of local boundary layer processes and long-range transport. *J. Geophys. Res.* 112, D13205. <https://doi.org/10.1029/2006JD008099>.
- Ojha, N., Naja, M., Singh, K.P., Sarangi, T., Kumar, R., Lal, S., Lawrence, M.G., Butler, T.M., Chandola, H.C., 2012. Variabilities in ozone at a semi-urban site in the Indo-Gangetic Plain region: association with the meteorology and regional process. *J. Geophys. Res.* 117, D20301. <https://doi.org/10.1029/2012JD017716>.
- Padhy, P.K., Varshney, C.K., 2000. Total non-methane volatile organic compounds (TNMVO) in the atmosphere of Delhi. *Atmos. Environ.* 34, 577–584. [https://doi.org/10.1016/S1352-2310\(99\)00204-6](https://doi.org/10.1016/S1352-2310(99)00204-6).
- Palmer, P.I., Jacob, D.J., Fiore, A.M., Martin, R.V., Chance, K., Kurosu, T.P., 2003a. Mapping isoprene emissions over North America using formaldehyde column observations from space. *J. Geophys. Res.* 108 (D6), 4180. <https://doi.org/10.1029/2002JD002153>.
- Pathak, B., Subba, T., Dahutia, P., Bhuyan, P.K., Moorthy, K.K., Gogoi, M.M., Babu, S.S., Chutia, L., Ajay, P., Biswas, J., Barhali, C., Borgohain, A., Dhar, P., Guha, A., De, B.K., Banik, T., Chakraborty, M., Kundu, S.S., Singh, S.B., Sudhakar, S., 2016. Aerosol characteristics in North-East India using ARFINET spectral optical depth measurements. *Atmos. Environ.* 125, 461–473. Part B. <https://doi.org/10.1016/j.atmosenv.2015.07.038>.
- Piccot, S.D., Watson, J.J., Jones, J.W., 1992. A global inventory of volatile organic compound emissions from anthropogenic sources. *J. Geophys. Res. Atmos.* 97, 9897–9912. <https://doi.org/10.1029/92JD006682>.
- Placet, M., Mann, C.O., Gilbert, R.O., Niefer, M.J., 2000. Emissions of ozone precursors from stationary sources: a critical review. *Atmos. Environ.* 34, 2183–2204. [https://doi.org/10.1016/S1352-2310\(99\)00464-1](https://doi.org/10.1016/S1352-2310(99)00464-1).
- Pozzer, A., Pollmann, J., Taraborrelli, D., Jockel, P., Helmig, D., Tans, P., Hueber, J., Lelieveld, J., 2010. Observed and simulated global distribution and budget of atmospheric C2–C5 alkanes. *Atmos. Chem. Phys.* 10, 4403–4422. <https://doi.org/10.5194/acp-10-4403-2010>.
- Priyadharshini, B., Verma, S., Giles, D.M., Holben, B.N., 2018. Discerning the pre-monsoon urban atmosphere aerosol characteristic and its potential source type remotely sensed by AERONET over the Bengal Gangetic plain. *Environ. Sci. Pollut. Res. Int.* 25, 22163–22179.
- Rumchev, K., Brown, H., Spickett, J., 2007. Volatile organic compounds: do they present a risk to our health? *Rev. Environ. Health* 22, 39–56.
- Sahu, L.K., Yadav, R., Pal, D., 2016. Source identification of VOCs at an urban site of western India: effect of marathon events and anthropogenic emissions. *J. Geophys. Res. Atmos.* 121, 2416–2433. <https://doi.org/10.1002/2015JD024454>.
- Sahu, L.K., Sheel, V., Pandey, K., Yadav, R., Saxena, P., Gunthe, S., 2015. Regional biomass burning trends in India: analysis of satellite fire data. *J. Earth Syst. Sci.* 124 (7), 1377–1387.
- Sahu, L.K., Lal, S., 2006b. Characterization of C2–C4 NMHCs distributions at a high altitude tropical site in India. *J. Atmos. Chem.* 54, 161–175. <https://doi.org/10.1007/s10874-006-9023-0>.
- Sahu, L.K., Lal, S., 2006a. Distributions of C2–C5 NMHCs and related trace gases at a tropical urban site in India. *Atmos. Environ.* 40, 880–889. <https://doi.org/10.1016/j.atmosenv.2005.10.021>.
- Sarangi, T., Naja, M., Lal, S., Venkataramani, S., Bhardwaj, P., Ojha, N., Kumar, R., Chandola, H.C., 2016. First observations of light non-methane hydrocarbons (C2–C5) over a high altitude site in the central Himalayas. *Atmos. Environ.* 125, 450–460. <https://doi.org/10.1016/j.atmosenv.2015.10.024>.
- Sarkar, C., Sinha, V., Kumar, V., Rupakheti, M., Panday, A., Mahata, K.S., Rupakheti, D., Kathayat, B., Lawrence, M.G., 2016. Overview of VOC emissions and chemistry from PTRTOF-MS measurements during the SusKat-ABC campaign: high acetaldehyde, isoprene and isocyanic acid in wintertime air of the Kathmandu Valley. *Atmos. Chem. Phys.* 16, 3979–4003. <https://doi.org/10.5194/acp-16-3979-2016>.
- Sarkar, S., Srivastava, R.K., Sagar, K., 2015. Diurnal monitoring of surface ozone and PM<sub>2.5</sub> concentration and its correlation with temperature. *Inter. J. Tech. Enhanc. Emerg. Eng. Res.* 3, 121–129.
- Sarkar, C., Chatterjee, A., Majumdar, D., Ghosh, S.K., Srivastava, A., Raha, S., 2014. Volatile organic compounds over Eastern Himalaya, India: temporal variation and source characterization using Positive Matrix Factorization. *Atmos. Chem. Phys. Discuss.* 14, 32133–32175. <https://doi.org/10.5194/acpd-14-32133-2014>.
- Sawyer, R.F., Harley, R.A., Cadle, S.H., Norbeck, J.M., Slott, R., Bravo, H.A., 2000. Mobile sources critical review: 1998 NARSTO assessment. *Atmos. Environ.* 34, 2161–2181. [https://doi.org/10.1016/S1352-2310\(99\)00463-X](https://doi.org/10.1016/S1352-2310(99)00463-X).
- Schell, B., Ackermann, I.J., Hass, H., Binkowski, F.S., Ebel, A., 2001. Modeling the formation of secondary organic aerosol within a comprehensive air quality model system. *J. Geophys. Res. Atmos.* 106, 28275–28293. <https://doi.org/10.1029/2001JD000384>.
- Seinfeld, J.H., Pandis, S.N., 2006. *Atmospheric Chemistry and Physics: from Air Pollution to Climate Change*, second ed. John Wiley & Sons, New York.
- Sharma, A., Ojha, N., Pozzer, A., Mar, K.A., Beig, G., Lelieveld, J., Gunthe, S.S., 2017. WRF-Chem simulated surface ozone over south Asia during the pre-monsoon: effects of emission inventories and chemical mechanisms. *Atmos. Chem. Phys.* 17, 14393–14413. <https://doi.org/10.5194/acp-17-14393-2017>.
- Sillman, S., 1995. The use of NO<sub>y</sub>, H<sub>2</sub>O<sub>2</sub> and HNO<sub>3</sub> as indicators for ozone-NO<sub>x</sub>-hydrocarbon sensitivity in urban locations. *J. Geophys. Res.* 100, 14175–14188.
- Sinha, V., Kumar, V., Sarkar, C., 2014. Chemical composition of pre-monsoon air in the Indo-Gangetic Plain measured using a new air quality facility and PTR-MS: high surface ozone and strong influence of biomass burning. *Atmos. Chem. Phys.* 14, 5921–5941. <https://doi.org/10.5194/acp-14-5921-2014>.
- Srivastava, P.K., Pandit, G.G., Sharma, S., Mohan Rao, A.M., 2000. Volatile organic compounds in indoor environments in Mumbai India. *Sci. Total Environ.* 255 (1–3), 161–168. [https://doi.org/10.1016/S0048-9697\(00\)00465-4](https://doi.org/10.1016/S0048-9697(00)00465-4).
- Stockwell, W.R., Middleton, P., Chang, J.S., Tang, X., 1990. The second generation regional acid deposition model chemical mechanism for regional air quality modeling. *J. Geophys. Res.* 95, 16343. <https://doi.org/10.1029/JD095iD10p16343>.
- Talapatra, A., Srivastava, A., 2011. Ambient air non-methane volatile organic compound (NMVOC) study initiatives in India - a review. *J. Environ. Prot.* 2 (1), 21–36. <https://doi.org/10.4236/jep.2011.21003>.
- Venkanna, R., Nikhil, G.N., Sinha, P.R., Siva Rao, T., Swamy, Y.V., 2015. Significance of volatile organic compounds and oxides of nitrogen on surface ozone formation at semi-arid tropical urban site, Hyderabad, India. *Air Qual. Atmos. Health* 9 (4), 379–390. <https://doi.org/10.1007/s11869-015-0347-2>.
- Verma, S., Reddy, D.M., Ghosh, S., Kumar, D.B., Chowdhury, A.K., 2017. Estimates of spatially and temporally resolved constrained black carbon emission over the Indian region using a strategic integrated modeling approach. *Atmos. Res.* 195, 9–19. <https://doi.org/10.1016/j.atmosres.2017.05.007>.
- Volkamer, R., Molina, L.T., Molina, M.J., Shirley, T., Brune, W.H., 2005. Doas

- measurement of glyoxal as an indicator for fastvoc chemistry in urban air. *Geophys. Res. Lett.* 32, L08806. <https://doi.org/10.1029/2005GL022616>.
- Vrekoussis, M., Wittrock, F., Richter, A., Burrows, J.P., 2010. GOME-2 observations of oxygenated VOCs: what can we learn from the ratio glyoxal to formaldehyde on a global scale? *Atmos. Chem. Phys.* 10, 10145–10160. <https://doi.org/10.5194/acp-10-10145-2010>.
- Vrekoussis, M., Wittrock, F., Richter, A., Burrows, J.P., 2009. Temporal and spatial variability of glyoxal as observed from space. *Atmos. Chem. Phys.* 9 (13), 4485–4504. <https://doi.org/10.5194/acp-9-4485-2009>.
- Wiedinmyer, C., Akag, S.K., Yokelson, R.J., 2011. The Fire Inventory from NCAR (FINN): a high resolution global model to estimate the emissions from open burning. *Geosci. Model Dev.* 4, 625–641. <https://doi.org/10.5194/gmd-4-625-2011>.
- Wolfe, G.M., Kaiser, J., Hanisco, T.F., Keutsch, F.N., de Gouw, J.A., Gilman, J.B., Graus, M., Hatch, C.D., Holloway, J., Horowitz, L.W., Lee, B.H., Lerner, B.M., Lopez-Hilfiker, F., Mao, J., Marvin, M.R., Peischl, J., Pollack, I.B., Roberts, J.M., Ryerson, T.B., Thornton, J.A., Veres, P.R., Warneke, C., 2016. Formaldehyde production from isoprene oxidation across NO<sub>x</sub> regimes. *Atmos. Chem. Phys.* 16, 2597–2610. <https://doi.org/10.5194/acp-16-2597-2016>.